https://doi.org/10.5194/egusphere-2026-367
Preprint. Discussion started: 8 May 2026

Forest and bioenergy expansion amplifies climate warming by accelerating regional cloud loss

Nanjian Liu[1,3], Zhixin Hao[*1,3], Siyou Xia[4], Peng Zhao[2,3]

1. Institute of Geographic Sciences and Natural Resources Research, Chinese Academy of Sciences, Beijing 100101, China

2. State Key Laboratory of Mountain Hazards and Engineering Safety, Institute of Mountain Hazards and Environment, Chinese Academy of Sciences, Chengdu 610299, China

3. University of Chinese Academy of Sciences, Beijing 100049, China

4. Department of Geography, University at Buffalo-SUNY, Buffalo 14261, USA

* Corresponding author: haozx@igsnrr.ac.cn.

Abstract

Land use and land cover change (LUCC) can exacerbate cloud-mediated climate warming. However, the long-term response of cloud cover to LUCC remains underexplored, particularly regarding differences between idealized and realistic forest expansion scenarios, as well as between forest and bioenergy expansion. Here, using simulations from the fully coupled Community Earth System Model (CESM), we demonstrate that large-scale idealized afforestation and bioenergy expansion accelerate the loss of low- and mid-level clouds while enhancing high-level clouds, thereby amplifying regional warming hotspots through intensified positive shortwave cloud radiative forcing. In contrast, realistic afforestation yields a net cooling effect. Idealized afforestation drives a

https://doi.org/10.5194/egusphere-2026-367
Preprint. Discussion started: 8 May 2026

pronounced decline in low-level cloud cover (1.14 times globally, 1.52 times over land), followed by bioenergy expansion (1.03 times globally and 1.23 times over land), primarily driven by reduced total precipitable water and relative humidity, as revealed by an interpretable machine learning framework, which identifies biophysical warming of the boundary layer due to albedo-driven surface heating and enhanced sensible heat flux as the dominant mechanism. Forest darkening reduces surface albedo, which increases absorbed solar radiation and elevates sensible heat, thereby drying the boundary layer and suppressing cloud formation. Conversely, realistic afforestation mitigates the loss of low- and mid-level clouds and suppresses boreal warming. Our findings indicate that more forest expansion does not always generate greater climate benefits; the climatic outcome largely depends on the type of land conversion and specific latitude bands, and highlights the critical importance of carefully selecting afforestation areas in the future to achieve positive climate benefits.

Keywords: Land use change; afforestation; bioenergy; cloud trend; climate warming

1. Introduction

Large-scale atmospheric circulation systems on Earth directly facilitate cloud formation through thermodynamic uplift and cooling mechanisms (Boucher et al., 2013; Klein et al., 2017; Nomokonova et al., 2020). Clouds play a crucial role in modulating the radiative energy balance at the top of the atmosphere (TOA) and the Earth's surface, with their impacts indirectly linked to temperature variations (Boehm and Thompson. 2023). For instance, low-level clouds, characterized by high albedo and significant optical depth, exert a substantial net cooling effect by reducing surface solar irradiance. In contrast, optically thinner high-altitude clouds, with an albedo approximately one-eighth that of low

https://doi.org/10.5194/egusphere-2026-367
Preprint. Discussion started: 8 May 2026

clouds, frequently induce net positive radiative forcing (Liou and Ou. 1983). The modulation of radiative balance and temperature by clouds is profoundly contingent upon their physical attributes, including type, thickness, liquid water path, and the dimensions of constituent particles (Albrecht et al., 1989; Stephens, 2005). The characteristics of cloud cover make it possible for them to play an amplifying role in climate warming (Ceppi and Nowack, 2021; Liu et al., 2025).

Clouds have been demonstrated to exert positive cloud feedback in nearly all climate models (Kiehl. 2007; Zelinka et al., 2017). Recent studies integrating satellite observations substantiate this assertion, revealing that cloud belts in equatorial and mid-latitude regions are contracting at a rate of 1.5-3% per decade (Tselioudis et al., 2025). This subtle disparity between incident and reflected radiation, arising from variations in cloud fraction, exacerbates Earth's planetary energy imbalance and amplifies climate warming (Li et al., 2024; Luo et al., 2024; Mauritsen et al., 2025; Shi et al., 2025). Further evidence indicates that the diminution of low-level cloud cover in certain regions during the initial two decades of the 21st century has directly intensified anomalous regional temperature elevations, thereby facilitating the emergence of new climate warming hotspots (Tselioudis et al., 2024; Tselioudis et al., 2025). Contemporaneous investigations elucidate that the recent widening of Earth's energy imbalance gap and unprecedented temperature highs are attributable to a marked decline in low-level cloud cover (Loeb et al., 2024; Goessling et al., 2025), with the underlying driver of cloud cover decrease being the escalation of greenhouse gas emissions from anthropogenic activities (Luo et al., 2024). Among these, land use changes since the Industrial Revolution have contributed approximately one-third of the greenhouse warming through the emission of greenhouse gases (Houghton, 2002;

https://doi.org/10.5194/egusphere-2026-367
Preprint. Discussion started: 8 May 2026

Goldewijk et al., 2004; Foley et al., 2005; van der Werf et al., 2009; Hong et al., 2021). Nevertheless, it remains unknown whether shifts in surface land cover types will render clouds less climatically beneficial and contribute to the formation of new warming hotspots.

Large-scale land use and land cover change (LUCC) is altering circulation patterns in local and remote regions (Portmann et al., 2024). Forests, as a common form of land cover, are highly favored in absorbing atmospheric CO_2 and mitigating climate warming (Peng et al., 2014). Changes in forests have been observed to exhibit significant interactions in heat fluxes and moisture between the surface and atmosphere from annual to seasonal scales; alterations in turbulence and water cycles will inevitably disrupt the atmospheric background for cloud formation and may reshape climate warming hotspots (Cheng et al., 2024). For instance, darker-colored forests absorb more solar radiation, leading to increased local radiation, whereby the absorbed additional energy is partitioned into sensible heat flux to heat the surface and the atmospheric temperature at the bottom of the boundary layer; this absorbed heat promotes the evaporation of surface and atmospheric moisture, thereby facilitating the development of shallow cumulus clouds (Ek and Holtslag. 2004). Compared to other vegetation, forests possess larger leaf area index (LAI) (Alkama and Cescatti. 2016), therefore, large-scale forest expansion enhances evapotranspiration by replacing croplands or grasslands, elevating atmospheric water vapor content and optimizing condensation environments, thereby increasing cloud cover and mitigating regional warming effects. Prior studies in Europe also indicate that forests overhead possess greater potential for cloud formation (Teuling et al., 2017). Another study on afforestation also demonstrates that the presence of forests augments low-level cloud amounts, and it is projected to yield positive climate benefits through such enhanced low-

https://doi.org/10.5194/egusphere-2026-367
Preprint. Discussion started: 8 May 2026

level cloud fraction; however, in regions with snow cover, this may result in diminished cloud amounts and engender converse climate effects (Duveiller et al., 2018; Duveiller et al., 2021; Breil et al., 2024).

Another distinctly divergent land use changes, namely the expansion of bioenergy crops, lacks the popularity of forests owing to its comparatively diminished CO_2 sequestration capacity, yet it can engender sufficiently substantial climate mitigation extents through biogeochemical and biogeophysical processes (Georgescu et al., 2011; Wang et al., 2021; Cheng et al., 2024). However, conversely, the cultivation of bioenergy crops may precipitate unintended ramifications, such as the depletion of deep soil moisture and the amplification of water resource deficits (Righelato and Spracklen, 2007; Cheng et al., 2022; Li et al., 2023), with these adverse effects typically manifesting more pronouncedly at regional scales than at global scales (Hallgren et al., 2013). In contradistinction to the elevated evapotranspiration rates of forests, low-transpiration bioenergy crops (such as switchgrass) commonly exhibit lower LAI, a physical attribute that may diminish the efficiency of moisture conveyance between the atmosphere and terrestrial surfaces, thereby impeding enhancements in atmospheric humidity and consequently precipitating reductions in local cloud cover (Bala et al., 2007). Both forest and bioenergy expansions exert varying degrees of influence on temperature, water cycles, and clouds through radiative and non-radiative processes; such influences may render the atmosphere more humid or arid across ranges extending hundreds of kilometers, thereby modulating cloud formation and subsequently reshaping the configuration of warming hotspots via cloud radiative effect (Cerasoli et al., 2021; Wang et al., 2021). Although the impacts of LUCC on atmospheric circulation play a pivotal role in projecting future climate

https://doi.org/10.5194/egusphere-2026-367
Preprint. Discussion started: 8 May 2026

changes and have been extensively investigated (Feddema et al., 2005; Swann et al., 2012; Li et al., 2018), comprehension of its effects on long-term trends in cloud cover remains largely unknown, particularly as the expansion of bioenergy has not received commensurate attention to that afforded to forest expansion. Therefore, it is entirely feasible to advance reasonable hypotheses positing that LUCC affects the generation and trends of local or remote cloud cover through complex or straightforward mechanisms (Hua et al., 2023).

We hypothesize that future large-scale LUCC scenarios will significantly modulate cloud cover trajectories through complex biogeophysical feedback. To test this, we utilized the Community Earth System Model (CESM) to perform fully coupled simulations from 2015 to 2100. Our results demonstrate that while realistic afforestation may offer regional climate benefits, idealized large-scale forest and bioenergy expansion could exacerbate the decline of mid-to-low-level clouds while accelerating the increase of high-level clouds. These structural shifts in cloud cover amplify shortwave radiative forcing, thereby intensifying the formation of regional warming hotspots. These findings suggest that future land-management strategies may inadvertently diminish the climatic cooling capacity of cloud systems.

2. Data and Methods

2.1. Data

The data used to validate the CESM model's capabilities comes from ECMWF Reanalysis v5 (ERA5), downloaded from the Copernicus Climate Service (https://cds.climate.copernicus.eu/datasets) (Muñoz-Sabater et al., 2021). National Centers for Environmental Prediction (NCEP) temperature, used to validate the simulation

https://doi.org/10.5194/egusphere-2026-367
Preprint. Discussion started: 8 May 2026

performance of temperature, is available from https://psl.noaa.gov/. Finally, the core data in this study is the land use data from Land-Use Harmonization 2 (LUH2) (Hurtt et al., 2020), downloaded from https://svn-ccsm-inputdata.cgd.ucar.edu/trunk/inputdata/.

2.2. Earth system simulation

We conducted the online simulations with the Community Earth System Model (CESM, version 2.1.3, https://www.cesm.ucar.edu/models/cesm2) (Danabasoglu et al., 2020). As a state-of-the-art tool in climate prediction, this model faithfully reproduces twentieth-century climate dynamics and sea temperatures while excelling in projections of essential climate variables (Danabasoglu et al., 2020; Fasullo, 2020). Similar to earlier versions (Lin and Rood. 1997), the atmospheric and land-surface component of CESM employs the Lin-Rood Finite-Volume (FV) dynamical core, though notable improvements have been introduced in atmospheric physics (Lin and Rood. 1997). Compared to its predecessor, the FV1, the new generation FV mainly adjusted its cloud parameters (Zhu et al., 2022). CESM incorporates the Community Atmosphere Model Version 6 (CAM6) as its atmospheric component, offering a high-top option (with 70 pressure levels reaching ~130 km) and a standard option (with 32 pressure levels reaching ~40 km). In this study, we utilize the standard low-top setup, which effectively simulates tropospheric atmospheric processes. CAM6 describes the atmospheric motion by the dynamics and sub-grid precipitation, cloud, and turbulence processes by the physics (Worley et al., 2011). Of particular relevance to our study is enhanced cloud-microphysics parameterization in CAM6: the Morrison-Gettelman 2 (MG2) scheme, which overcomes the prior constraint by explicitly predicting raindrop and snow-particle sizes (Morrison and Gettelman. 2008; Gettelman and Morrison. 2015). Accompanying enhancements feature the consolidated

https://doi.org/10.5194/egusphere-2026-367
Preprint. Discussion started: 8 May 2026

turbulence parameterization, incorporating a multivariate binormal probability density function (PDF) to collectively depict sub-grid fluctuations in temperature, humidity, and vertical velocity (Larson. 2017). At the same time, CESM classifies clouds across altitudes according to their cloud top pressure, delineating low-level cloud from 700 hPa to the surface, middle-level cloud from 700–400 hPa, and high-level cloud above 400 hPa (Danabasoglu et al., 2020).

Before launching the simulations, we first evaluated the performance of CESM to reproduce historical climate change. The historical run employed the BHIST compset and was carried out online at 1°×1° resolution. Monthly output in the period of 1979–2014 were used for model validation; to match the model grid, all observational datasets were conservatively interpolated to the CESM resolution. Annual and seasonal evaluations of temperature and cloud fraction show that CESM satisfactorily captures present-day climate variability (Figs. S24–S27). Then, the specific simulation design is implemented in the Community Land Model Version 5 (CLM5) within CESM. Relative to its predecessors, CLM5 incorporates advances in soil hydrology, crop modeling, fire feedbacks, and biogeochemical cycling, thereby enhancing the representation of anthropogenic land-use change within the climate system (Swenson and. Lawrence. 2012; Li et al., 2017; Levis et al., 2018; Lawrence et al., 2019). The idealized simulation experiments in this study were all conducted based on Land-Use Harmonization 2 (LUH2) (Hurtt et al., 2020). CLM represents land-surface heterogeneity through a nested sub-grid hierarchy, allowing multiple land-unit to coexist within each grid cell (Oleson et al., 2013). Although CLM is not configured with a dynamic vegetation model, the time-varying landuse.timeseries

https://doi.org/10.5194/egusphere-2026-367
Preprint. Discussion started: 8 May 2026

dataset provided by the model allows vegetation's physiological processes (such as photosynthesis, transpiration, etc.) to be explicitly simulated (Lawrence et al., 2019).

According to the FAO definition of afforestation, it refers to the establishment of new forests on land that was not previously classified as forest through planting or deliberate seeding. This implies a fundamental change in land use, for instance, from cropland to forest or from grassland to forest (FAO. 2012). Therefore, in our simulation experiments, we followed the FAO definition to construct idealized datasets for forest and bioenergy crop expansion. In CLM5, there are eight tree plant functional types (PFTs), indexed from 1 to 8, and 64 crop functional types (CFTs). In CLM5, PFTs and CFTs coexist on nested sub-grid tiles that jointly mediate energy and moisture exchanges between the land surface and the atmosphere. We therefore implement forest and bioenergy expansion by altering their fractional areas at the sub-grid scale. Specifically, our simulation experiments comprise a control run (CTL) in which land-cover fractions are held constant at 2015 levels, an idealized 50 % linear afforestation scenario (AF50), an idealized 50 % bioenergy crop expansion scenario (BE50), and a realistic forest expansion scenario (REAL) derived from previous studies (Roe et al., 2021; King et al., 2024; Weber et al., 2024), this land-use pathway exhibits a maximum 26 % forest-expansion pattern by 2100. All future-period simulations were conducted with the scientifically validated BSSP126 compset at 1°×1° (f09_g17_gl4) horizontal resolution, while the ocean component was run at 0.5° resolution, the restart files for model initialization are derived from the National Center for Atmospheric Research's 500-year equilibrated control simulation during the Industrial Revolution period. In the idealized simulations, forest expansion is restricted to shrubland and grassland, with the newly forested area distributed evenly among the eight tree PFTs;

https://doi.org/10.5194/egusphere-2026-367
Preprint. Discussion started: 8 May 2026

bare ground is excluded, although some recent studies (Liang et al., 2025) advocate afforestation on bare soil. Bioenergy expansion is represented by rained and irrigated sugarcane and occupies only existing bioenergy land, thereby encroaching neither on forests nor on natural grasslands (Fig. S23). This means that the simulated climate response originates entirely from biophysical processes triggered by land cover change (such as changes in albedo and evapotranspiration), excluding the offsetting effect of biogeochemical feedback (i.e., carbon sequestration) on short-term warming. The climatic response is quantified as the difference between each sensitivity experiment and the CTL, with statistical significance assessed using a two-tailed *Student's t* test.

2.3. Attribution of LUCC-induced atmospheric changes to cloud trends

In this study, to analyze the driving factors of cloud trends caused by different LUCC, we apply the explainable Extreme Gradient Boosting (XGBoost) model developed by Chen and Guestrin. (2016), whose proven capacity to capture nonlinear interactions and deliver high predictive skill has made it a workhorse in both atmospheric and ecological modelling (Ren et al., 2024; Flora et al., 2024). After model training, we use the SHapley Additive exPlanations (SHAP) method, based on game theory (Lundberg and Lee. 2017; Lundberg et al., 2020), to uncover the contributions and dependencies of key variables to cloud trends. Specifically, we constructed twelve models for the cloud and climate-change trends driven by LUCC and performed 100 times Bayesian hyperparameter searches (Snoek et al., 2012) and the optimized parameters name and the obtained best values are listed in Table S1.

2.4. Calculation of cloud radiative effect

Cloud radiative effect (CRE) is commonly used to evaluate the cooling or warming influence of clouds on the atmosphere (Goldblatt et al., 2021; Luo et al., 2024), measured

https://doi.org/10.5194/egusphere-2026-367
Preprint. Discussion started: 8 May 2026

at the top of the atmosphere, in the atmosphere, or at the surface (Zhang et al., 2022), which consists of shortwave CRE (swCRE), longwave CRE (lwCRE) and netCRE (the sum of swCRE and lwCRE). LwCRE was calculated as the difference between downward longwave radiation at the surface under cloudy conditions and that under clear sky. SwCRE is determined by the difference between downwelling solar flux at surface (FSDS) and clear-sky downwelling solar flux at surface (FSDSC), as well as upward shortwave radiation at the surface (FSUS) and clear-sky (FSUSC), as indicated in eq. (1).

$$\mathrm{swCRE} = \mathrm{FSDS} - \mathrm{FSDSC} - \mathrm{FSUS} + \mathrm{FSUSC} \quad (1)$$

In eq. (1), FSUS and FSUSC are indirectly calculated via FSDS and FSDSC multiply albedo, as shown in eq. (2). FSNS denotes the net shortwave radiation at the surface. The clear-sky albedo is also calculated using a similar equation.

$$\mathrm{Albedo} = 1 - \left(\frac{\mathrm{FSNS}}{\mathrm{FSDS}}\right) \quad (2)$$

2.5. Quantifying the impacts of land use change

In this study, the impact of land use change on climate system is quantified as the difference between the control and sensitivity experiments, denoted by the symbol Δ. Using CLDTOT as an example, the effect of land use change on CLDTOT is defined by eq. (3).

$$\Delta\mathrm{CLDTOT} = \mathrm{AF50} - \mathrm{CTL} \quad (3)$$

2.6. Pixel-based linear trend

In this study, we conducted ordinary least squares (OLS) fitting through simple linear regression on every grid point to investigate the temporal variability patterns of atmospheric variables, encompassing cloud cover. The significance of linear trend and sensitivity for each grid was derived from *Student's t* test, as expressed in eq.(4).

https://doi.org/10.5194/egusphere-2026-367
Preprint. Discussion started: 8 May 2026

$$S = \frac{\sum_{t=1}^{n}\left(x_{t,i,j} - \bar{x}_{i,j}\right)\left(y_{t,i,j} - \bar{y}_{i,j}\right)}{\sum_{t=1}^{n}\left(x_{t,i,j} - \bar{x}_{i,j}\right)^2} \quad (4)$$

2.7. Quantification of the inequality of cloud trends

The Gini coefficient (Gini index) is most often used in economics to measure the state of socio-economic development, and we use it here to analyze the hemispheric inequality of the cloud trend. The continuous equation for the Gini index is shown in eq.(5).

$$\text{Gini index} = 1 - 2\int_0^1 L(x)dx \quad (5)$$

Here, the Gini index is derived through the integration of the area beneath the Lorenz curve L(x), serving to quantify the cumulative proportion of the target variable relative to the total proportion.

2.8. Surface energy balance decomposition of temperature

To better reveal the impacts of LUCC at different scales on surface thermodynamic temperature, this study employs the energy balance equation to dissect the various physical components of temperature changes. Through this method, the surface temperature changes caused by afforestation and bioenergy expansion can be attributed to multiple direct or indirect biophysical processes. Previous studies have shown that the linear approximation method via first-order Taylor expansion is sufficiently accurate for assessing surface temperature anomalies induced by large-scale land cover changes (Lee et al., 2011; Devaraju et al., 2018; Chen et al., 2020; Sui et al., 2025). According to the principle of energy conservation, the radiation energy absorbed by the surface must equal the heat released, as described in eq. (6).

$$(1 - \alpha_s)SW_{\downarrow} + LW_{\downarrow} - \varepsilon\sigma T_s^4 = H + LE + G \quad (6)$$

https://doi.org/10.5194/egusphere-2026-367
Preprint. Discussion started: 8 May 2026

In eq.(6), α_s represents surface albedo, and $SW_{\downarrow}$ denotes downward shortwave radiation; thus, $(1-\alpha_s)SW_{\downarrow}$ represents net shortwave radiation at the surface. LW denotes downward longwave radiation from the surface. ε is surface emissivity, a parameter used to describe how closely the Earth approximates a perfect blackbody, with typical values less than 1 (0.7 in this study). σ is the Stefan-Boltzmann constant ($5.671*10^{-8}$W/m^2/K^4). H represents sensible heat flux, LE represents latent heat flux, T_s is surface temperature, and G is surface heat flux (this value typically varies very little and can therefore be neglected in calculations). Rearranging and transforming the equation yields eq. (7), where ρ is air density (1.29 kg/m^3), C_p is specific heat capacity (1030 J/kg/K), r_a is aerodynamic resistance (s/m), T_a is air temperature at 2 meters, and β represents the Bowen ratio.

$$\varepsilon\sigma T_s^4 = (1-\alpha_s)SW_{\downarrow} + LW_{\downarrow} - \frac{(1+\beta)}{\beta}\frac{\rho C_p}{r_a}(T_s - T_a) \quad (7)$$

Linearizing eq.(7) yields the difference in surface temperature changes ΔT_s between the sensitivity experiment and the CTL experiment. After linear decomposition, the equation allows the surface temperature change to be explicitly expressed as a function of albedo (α_s), turbulent processes (β), surface roughness or aerodynamic resistance (r_a), cloud radiation effects ($LW_{\downarrow}$ and $SW_{\downarrow}$), and atmospheric feedback (T_a), as shown on the right-hand side (RHS) of eq.(8).

$$\Delta T_s = \left(\frac{-\lambda_0 SW_{\downarrow}}{1+f}\right)\Delta\alpha + \left[\frac{\lambda_0 H}{(1+f)\beta^2}\right]\Delta\beta + \left[\frac{fH}{(1+f)\rho C_p}\right]\Delta r_a + \left[\frac{\lambda_0(1-\alpha)}{1+f}\right]\Delta SW_{\downarrow} + \left(\frac{\lambda_0}{1+f}\right)\Delta LW_{\downarrow} + \left(\frac{f}{1+f}\right)\Delta T_a \quad (8)$$

In eq.(8), λ_0 and f represent the temperature sensitivity coefficient and the energy redistribution coefficient, respectively, as defined by eq.(9) and (10). These two parameters

https://doi.org/10.5194/egusphere-2026-367
Preprint. Discussion started: 8 May 2026

respectively describe the response of blackbody radiation to temperature and how turbulent fluxes regulate surface temperature.

$$\lambda_0 = \frac{1}{4\sigma\varepsilon T_s^3} \tag{9}$$

$$f = \frac{\rho C_p}{4\sigma\varepsilon T_s^3 r_a}\left(1 + \frac{1}{\beta}\right) \tag{10}$$

Finaly, we calculate the annual trend of each term using eq. (4). In this way, the long-term trends of each physical term induced by LUCC forcing can be investigated.

3. Results

3.1. Long-term response of cloud cover to LUCC forcings

Our simulations demonstrate that distinct land-use forcing significantly altered the global long-term trends in total cloud cover (CLDTOT) and low-level clouds (CLDLOW) (Figure 1). While CLDTOT exhibited a moderate negative trend in both CTL (-0.0083±1037%/year) and the bioenergy expansion experiment (BE50), the idealized (AF50) and realistic afforestation (REAL) scenarios modestly attenuated this decline, respectively. The most pronounced and contrasting response was simulated in CLDLOW. Idealized afforestation induced a rapid loss, representing an approximately 1.14 times increase in loss rate compared to the CTL simulation and this effect was particularly strong over land, where AF50 accelerated the decline rate by 1.52 times (Figure S1). This suggests that extensive afforestation may reduce low-level clouds by altering surface evapotranspiration and enhancing boundary layer stability, forming a negative feedback mechanism (Duveiller et al., 2021; Leung et al., 2024). In stark contrast, the realistic afforestation scenario suppressed the CLDLOW loss rate, while BE50 induced only a

https://doi.org/10.5194/egusphere-2026-367
Preprint. Discussion started: 8 May 2026

minimal loss rate (1.03 times, 1.23 times on land). In addition, all simulations suppressed the loss rate of low-level clouds over the ocean (Figure S1).

Medium-level clouds (CLDMED) exhibited a consistent downward response to land use forcings, with trends ranging from -0.0101±0.0864%/year in CTL to -0.0121±0.0873%/year in AF50, idealized scenarios (AF50 and BE50) induced slightly steeper trends. High-level clouds (CLDHGH) displayed positive trends across all land use forcing simulations, with slopes varying from 0.0053±0.1342%/year in CTL to 0.0082±0.1439%/year in AF50. This variation is largely dominated by large-scale thermodynamic forcing, as linear models for CLDHGH explained only 37%-46% of the variability (Figure 1m-p). Crucially, both idealized and realistic afforestation amplified this upward trend in CLDHGH. Compared to CTL, AF50 enhanced the increase by approximately 1.5 times (2.28 times on land and 1.41 times on ocean), and REAL enhanced it by about 1.3 times (2.17 times on land and 1.16 times on ocean). Ocean changes were generally insignificant, possibly due to the buffering effect of remote atmospheric transport (Portmann et al., 2022).

The robust amplification of the CLDHGH positive trend by afforestation, coupled with the acceleration of CLDLOW loss, highlights a critical trade-off in land-based climate mitigation. Prior analyses have demonstrated that greenhouse warming elevates high-level cloud top heights, thereby amplifying climate warming (Norris et al., 2016; Zelinka et al., 2016). Our findings indicate that large-scale afforestation in the future, particularly under idealized global implementation scenarios, could inadvertently intensify climate warming by amplifying the high-level cloud feedback mechanism. Moreover, the pronounced acceleration of low-level cloud depletion over land in the AF50 scenario suggests adverse

https://doi.org/10.5194/egusphere-2026-367
Preprint. Discussion started: 8 May 2026

surface biophysical feedback. Conversely, the minimal interference observed in the REAL scenario, which often slows cloud loss rates, is largely attributed to the strategically focused location of forest expansion (King et al., 2024; Weber et al., 2024), leading to cloud feedback closer to natural variability.

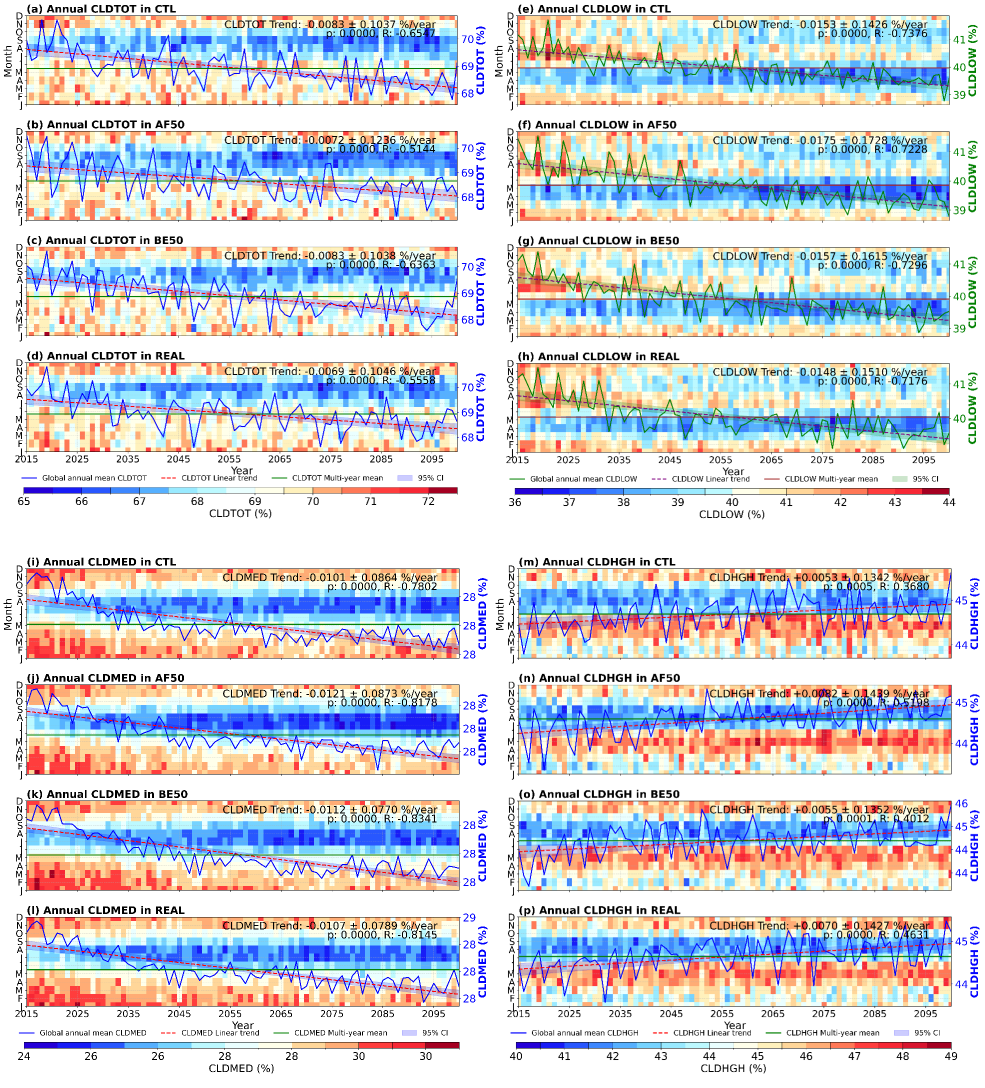

Figure 1. Long-term change and area-weighted global mean trends of cloud cover in different simulations. The shade indicates 95% confidence interval (CI). When

https://doi.org/10.5194/egusphere-2026-367
Preprint. Discussion started: 8 May 2026

subtracting from the CTL simulation results, the associated uncertainty was propagated using quadrature addition of standard errors (Taylor. 1997; Mastrandrea et al., 2010).

3.2. Spatial response of cloud cover to LUCC forcings

Distinct land use forcings exerted pronounced regional impacts on long-term cloud cover trends, exhibiting substantial geographic heterogeneity across hemispheres and between land and ocean areas (Figure 2, Figure S2-S5). Both afforestation and bioenergy expansion drove negative CLDTOT trends in the Northern Hemisphere (NH). Notably, BE50 induced the steepest overall decline (mean CLDTOT trend: -0.0045 %/year), accelerating the loss at a rate approximately 2.3 times that of AF50 (mean: -0.0019 %/year). However, the most striking feature was the intense, concentrated CLDLOW loss induced by AF50 (mean NH trend: -0.0060 %/year). Negative CLDLOW trends were strongly localized over mid-to-high latitude landmasses in North America and Eurasia, with the intensity of loss in these land regions being 20 times that of the overall Southern Hemisphere (SH). This phenomenon, indicative of exacerbated seasonal losses during summer, was also evident in BE50 and REAL simulations, suggesting a general latitude dependency (Figure 3, Figure S3-S4). Furthermore, CLDMED trends displayed regional divergence, with BE50 inducing CLDMED increases in Australia and Southeast Asia while AF50 amplified losses in those same regions.

At the global scale, both LUCC forcings led to a spatial contraction of regional cloud loss areas but, critically, an intensification of loss magnitudes (Figure S6). For instance, AF50 contracted the CLDTOT loss area by 6.01%, yet the intensity of losses within those areas increased significantly. This indicates that idealized afforestation does not produce a linear, uniform reduction in cloud cover globally, but rather concentrates climate damage

https://doi.org/10.5194/egusphere-2026-367
Preprint. Discussion started: 8 May 2026

in a few land regions highly sensitive to biophysical forcing, creating highly concentrated climate warming hotspots. Furthermore, both REAL and BE50 amplified CLDHGH increases over Australia, and REAL induced a more intense mean CLDHGH trend in the SH compared to AF50 (Figure S2g-h). These results suggest that realistic afforestation may also contribute to warming by accelerating CLDHGH increases over certain SH oceanic regions. Additionally, it is noteworthy that realistic afforestation significantly exacerbates the rate of low-level cloud loss on the western side of South America, even though the forest expansion in this scenario primarily occurs on the southeastern side of the region. However, this may lead to unexpected negative impacts on the climate of the other side, and this indicates that the cloud-mediated drought risks induced by land use changes may be particularly prominent here (Li et al., 2025).

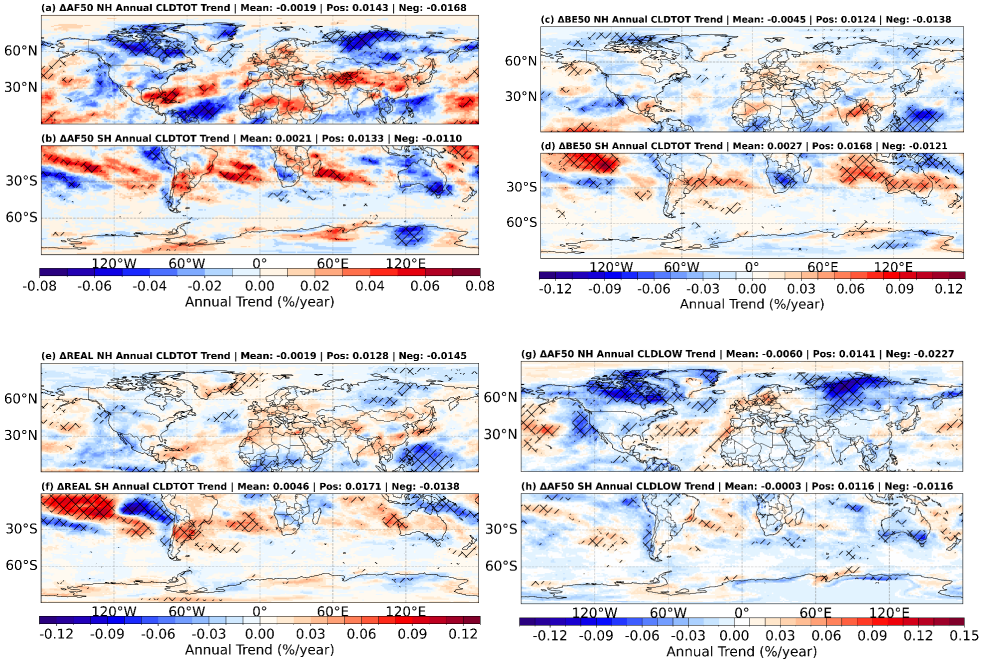

https://doi.org/10.5194/egusphere-2026-367
Preprint. Discussion started: 8 May 2026

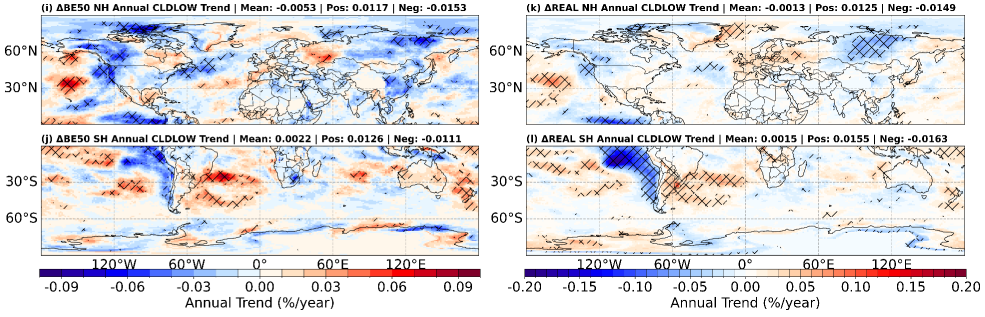

379

380 **Figure 2. Long-term spatial trends of total and low-level cloud cover induced by the**

381 **expansion of forest and bioenergy in Northern Hemisphere and Southern Hemisphere**.

382 The cross-hatching indicates the grids with a significant trend (p<0.05).

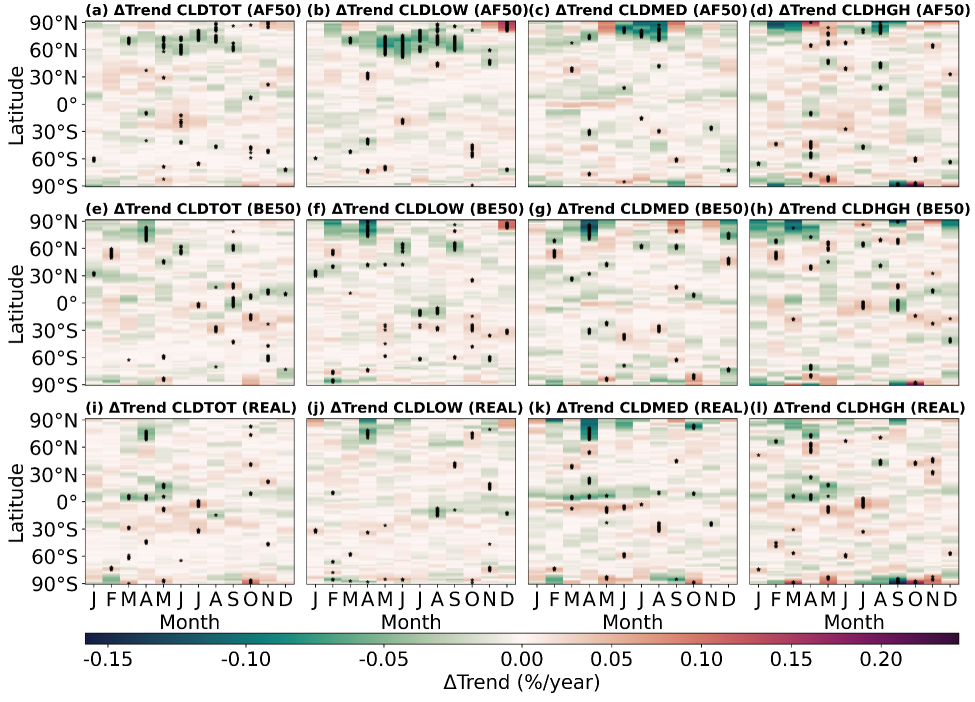

383

384 **Figure 3. Responses of cloud-cover trends to different land-use changes group by**

385 **month.** The black asterisk indicates the grids with a significant trend (p<0.05).

386 ## 3.3. The response of temperature and cloud radiative effect to LUCC

https://doi.org/10.5194/egusphere-2026-367
Preprint. Discussion started: 8 May 2026

Distinct land use forcings influence temperature trends and their spatial distribution primarily through cloud radiative effects (Schneider. 1972). While most regions show increasing thermodynamic temperature at 2 meter (TREFHT) trends across all simulations, idealized afforestation causes widespread warming and concentrates these trends into specific areas (Figure S9). The expansion of bioenergy crops substantially redistributes the warming hotspots induced by AF50, the intensity is alleviated in many regions (e.g., Southern Ocean, Antarctica), while opposite changes occur elsewhere, such as the Western Pacific, where BE50 reverses AF50's cooling to a warming trend. A similar redistribution of hotspots is observed when comparing AF50 with realistic afforestation; notably, REAL mitigates or offsets the significant warming trends seen in AF50 across mid-to-high latitudes of North America and Eurasia.

The mean latitudinal responses of TREFHT show a clear contrast (Figure 4d). AF50 induces substantial warming in mid-to-high latitudes of the NH, while REAL causes the greatest cooling trends there. This warming is amplified by accelerating cloud cover losses, primarily through enhanced positive swCRE trends from rapid low-level cloud loss (Figure 4, Figure 5, Figure S6-8). The regions with larger cloud loss magnitudes and stronger temperature rise trends largely overlap, particularly in the boreal region (50°N-90°N). Relative to the global average, AF50 and BE50 significantly amplified warming here (factors of 2.15 times and 1.71 times, respectively), while REAL induced cooling (factor of -1.51 times). This pronounced warming amplification phenomenon is primarily driven by an enhanced atmospheric feedback trend, further amplified by the accelerated reduction of clouds in the middle and low-level clouds (Figure 5). AF50 caused the low-level cloud loss rate in this region to be 8.80 times the global average, and BE50's relative amplification

https://doi.org/10.5194/egusphere-2026-367
Preprint. Discussion started: 8 May 2026

was even higher (13.63 times). Furthermore, the total cloud cover declines significantly contributed to the temperature rise, showing 8.88 times the global level in AF50 and a dramatic 26.12 times in BE50. Therefore, under the idealized LUCC scenario, the significant warming phenomenon simulated in the boreal region is partly attributed to the enhanced trend of swCRE caused by mid-to-low-level cloud loss, although atmospheric feedback plays a dominant role. A significantly enhanced trend in swCRE can be observed on the western side of South America, which is associated with accelerated loss of low-level clouds.

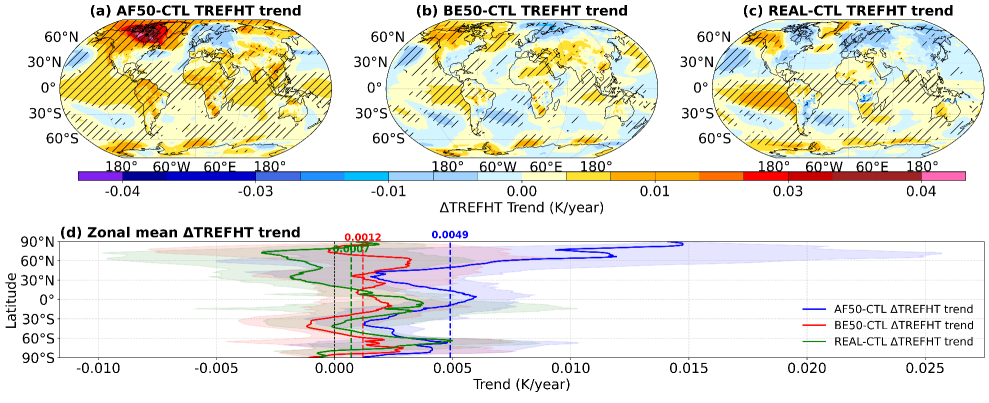

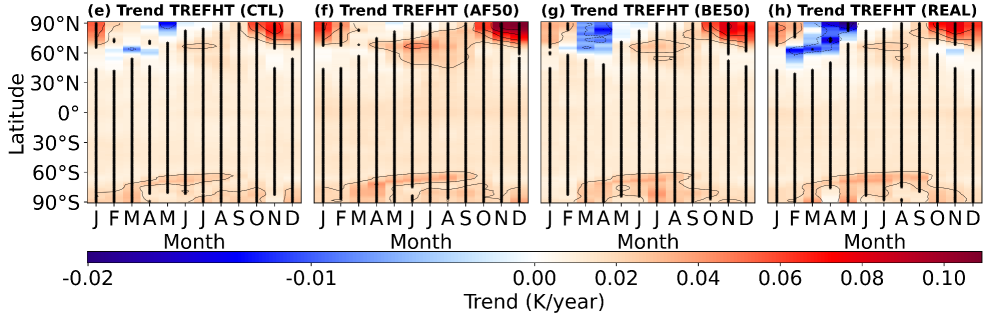

https://doi.org/10.5194/egusphere-2026-367
Preprint. Discussion started: 8 May 2026

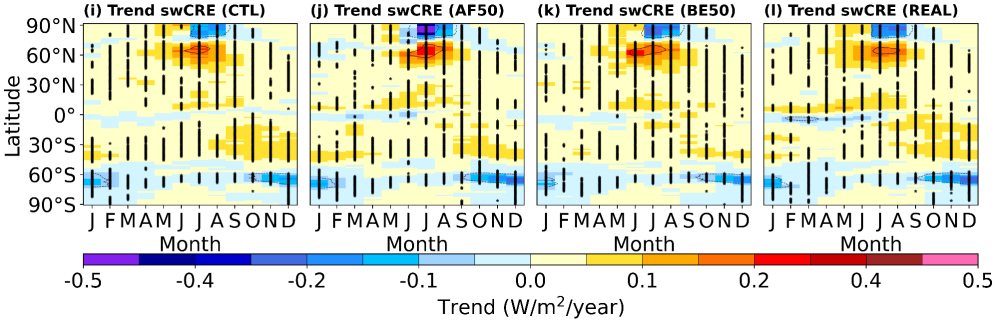

420

421 **Figure 4. Long-term trends of reference height temperature and cloud radiative effec**t.
422 (a-d) Spatial trends and mean zonal distribution of reference height temperature induced
423 by different land use and land cover change. (e-l) Trends in temperature and shortwave
424 cloud radiative effect (swCRE) grouped by month in different simulation experiments. An
425 enhanced positive trend in swCRE indicates that shortwave radiative cooling of clouds is
426 either weakening or amplifying warming. The black hatch and scatter indicate the grids
427 that passed the test of significance (p<0.05) and the shade in (d) indicates standard
428 deviation.

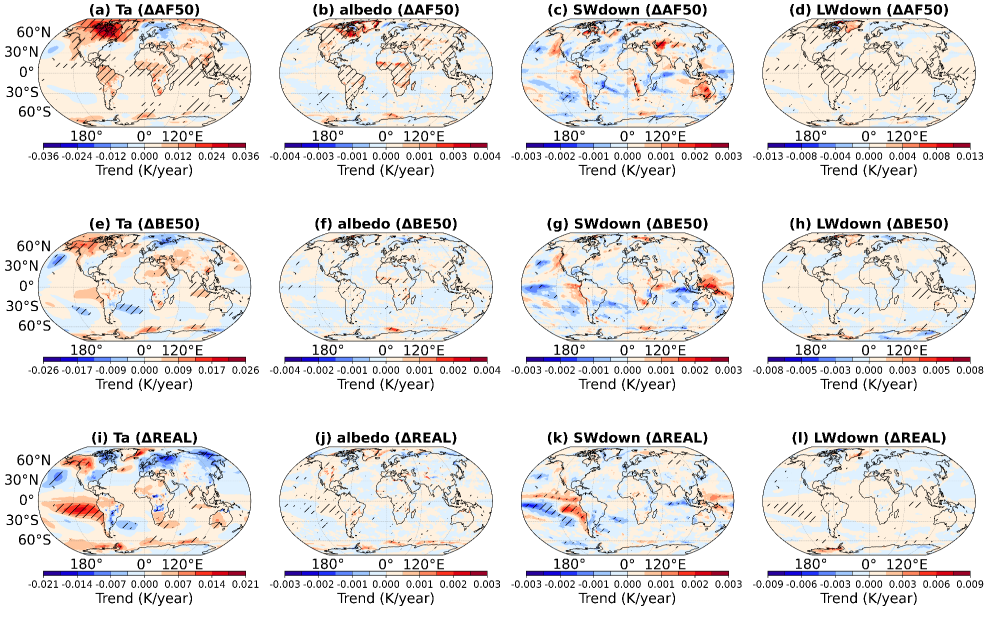

429
430
431

https://doi.org/10.5194/egusphere-2026-367
Preprint. Discussion started: 8 May 2026

Figure 5. Long-term trends of key physical terms (decomposed by the surface energy balance equation) induced by different LUCC. T_a represents the atmospheric feedback term, albedo denotes the surface albedo term, and SWdown and LWdown indicate the downward shortwave and longwave radiation terms, respectively. The black hatch indicates the grids that passed the test of significance (p<0.05).

3.4. Forest and bioenergy-induced hemispheric cloud trends asymmetry

We used the Gini index to quantitatively assess the inequality and spatial concentration of global cloud cover trends due to LUCC (Zhao et al., 2025). A Gini index closer to one signifies a highly unequal distribution, with trends strongly concentrated in specific latitude bands. For CLDTOT, idealized afforestation significantly intensified concentrated cloud losses in both hemispheres (e.g., SH downward trends Gini index rose from 0.48 to 0.52, Figure 6, Figure S10), suggesting amplified local land use impacts (Hua et al., 2023). This concentration effect was most dramatic for CLDLOW in the NH, where AF50 caused the Gini index to rise sharply from 0.41 (CTL) to 0.50, indicating a greater concentration of cloud decline areas (Figure S10f). Bioenergy expansion induced milder asymmetry overall, but still concentrated SH increases in specific CLDTOT and CLDHGH hotspots (Figure S11).

In stark contrast to idealized expansion, realistic afforestation consistently exerted the minimal influence on cloud trend heterogeneity, remaining closest to the CTL simulation (Figure S12). For CLDTOT, REAL slightly broadened NH increasing trends (Gini index: 0.54 to 0.50) with limited alteration to the overall spatial patterns. For CLDLOW, REAL increased the concentration of NH downward trends, but its impact was far less pronounced than that of AF50 (Gini: 0.41 to 0.43), this means that realistic afforestation will

https://doi.org/10.5194/egusphere-2026-367
Preprint. Discussion started: 8 May 2026

concentrate the loss of low-level clouds in specific areas. Overall, these results show that idealized LUCC forcings strongly alter inter-hemispheric cloud heterogeneity, inducing a concentrated loss of low-level clouds, a process that is highly disruptive to climate patterns, unlike the weaker and less spatially disruptive effects observed under realistic scenarios.

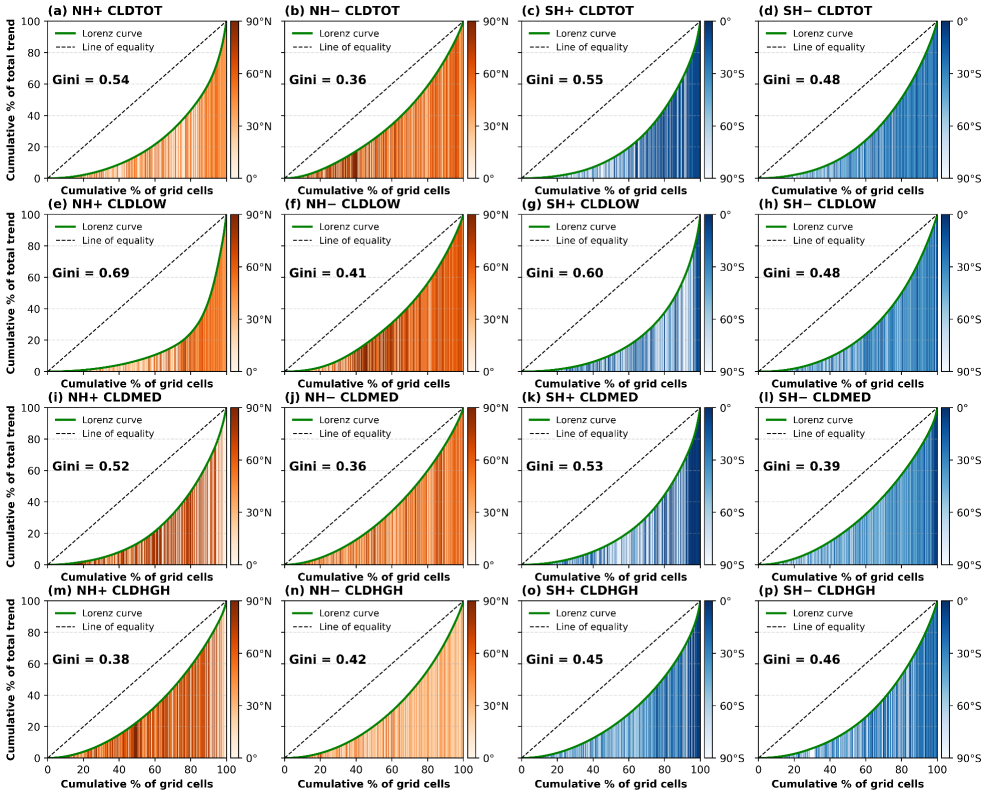

Figure 6. Asymmetry of cloud trends between hemispheres. Lorenz curves of long-term CLDTOT (a-d), CLDLOW (e-h), CLDMED (i-l), CLDHGH (m-p) trend in the Northern (0° to 90°N) and Southern Hemispheres (0° to 90°S) during the 2015–2100 in CTL run. The results of the AF50, BE50, and REAL experiments can be found in Figure S10-S12.

3.5. Possible physical mechanisms of cloud trends change revealed by machine learning

https://doi.org/10.5194/egusphere-2026-367
Preprint. Discussion started: 8 May 2026

The aforementioned analyses indicate that distinct LUCC significantly altered the geographic distribution of global cloud cover trends. We employed an interpretable machine learning model to further elucidate the underlying mechanisms and quantify their respective contributions.

Regarding the driving factors for the trend changes in CLDTOT, the trend changes in total precipitable water (TMQ) are the most important in all simulations, with contributions of 20.5%, 26.3%, and 23.1% in the AF50, BE50, and REAL, respectively (Figure 7); and the direction of influence remains basically consistent (Figure 8), meaning that the LUCC-induced TMQ decrease (increase) trend accelerates the loss (increase) rate of CLDTOT, which indicates that large-scale LUCC disturbances to the hydrological cycle are the primary macroscopic factor controlling long-term changes in total cloud cover (Pielke Sr et al., 2007). We also found that the dependence of AF50-induced TMQ on CLDTOT was significantly stronger than that of BE50 and REAL, and was approximately linear. The decreasing trend of TMQ directly drove the decreasing trend of CLDTOT (Figure 8a-c). However, the regulatory role of TMQ varies by location; the TMQ increase trend induced by idealized forest expansion mainly contributes to the CLDTOT increase trend in tropical regions, while outside the tropics, it is primarily negative contributions (Figure 9). These results indicate that the rapid loss of CLDTOT in the NH land areas observed in Figure 2 is attributed to the long-term loss of atmospheric moisture supply; the decrease in TMQ directly contributes to the atmosphere becoming drier. Particularly in water-limited regions of the mid- to high-latitudes of the Northern Hemisphere, the transpiration induced by forests replacing grasslands tends to be weak, which implies that the efficiency of water vapor transport from forests to the atmosphere is lower (Breil et al., 2021). The temperature

https://doi.org/10.5194/egusphere-2026-367
Preprint. Discussion started: 8 May 2026

rise and relative humidity decrease caused by AF50 are not limited to the surface. Simulations show that the warming and drying trends extend vertically through the troposphere (Figure 10). The decrease in relative humidity causes the lifting condensation level (LCL) of water vapor to rise. When the rising speed of the LCL exceeds the development speed of the boundary layer top, clouds cannot form, or are pushed to drier upper levels and dissipate (Romps. 2017; Kutta and Hubbart. 2023). This explains the mechanism by which AF50 leads to the synchronous loss of mesosphere clouds (accelerated by 1.25 times over land): thermodynamic disturbances at the land surface suppress moisture supply at vertical heights by affecting boundary layer height and stability, thereby inhibiting mesosphere cloud development. In contrast, the success of the REAL scenario lies in its ability to effectively optimize the heat distribution between the surface and the atmosphere, allowing atmospheric cooling and evapotranspiration efficiency to dominate, thus offsetting the warming effect caused by the decrease in albedo (Figure 10). Previous modeling studies have shown that progressive afforestation in midlatitudes may suppress moisture supply, thereby causing tropospheric drying; the reduction in cloud fraction across vertical levels is precisely the result of this atmospheric response (Laguë and Swann. 2016). Therefore, in the idealized afforestation simulation, changes in relative humidity can be seen as the second largest driving factor, contributing to 14.1%. This attribution also applies to the regional CLDTOT losses caused by bioenergy crop expansion and realistic afforestation, with only slight differences in the aspect of the second largest driving factor.

For the attribution of the CLDLOW trend, relative humidity becomes the most important contributing factor, with contributions induced by AF50, BE50, and REAL being

https://doi.org/10.5194/egusphere-2026-367
Preprint. Discussion started: 8 May 2026

20.4%, 20.4%, and 15.3% respectively, among which the relative humidity decline trend induced by idealized afforestation leads to the most severe CLDLOW loss rate, and this impact is mainly concentrated in the mid-to-high latitude regions of the NH (Figure S15a). At the same time, this simulation induces a significant increase in maximum temperature in response to the substantial and rapid loss of CLDLOW (Figure S20e), which indicates that the relative humidity decline, and maximum temperature rise trends induced by idealized afforestation jointly amplify the loss rate of CLDLOW, and it exhibits a strong linear dependency (Figure S14a-b). Afforestation in the mid-to-high latitude regions of the NH causes the surface in these areas to darken, leading to a decrease in albedo, thereby increasing the absorption of solar radiation to raise surface temperature (Meissner et al., 2003; Swann et al., 2010), and the amount of albedo reduction per unit afforestation in these regions and the increased radiative forcing are much higher than in other regions (Foley et al., 1994; Weber et al., 2024). The simulation proves that the regions with rapid decline in CLDLOW induced by idealized afforestation simultaneously experience rapid rise in maximum temperature and rapid decline in relative humidity. Albedo is the main biophysical source affecting temperature changes in the NH land areas (Arora and Montenegro. 2011), but it is unlikely to directly induce long-term loss of cloud cover; the missing bridge in between needs to be supplemented by water vapor supply, therefore relative humidity is parsed by the machine learning model as the most important driving factor for the accelerated loss of CLDLOW, with maximum temperature following closely behind.

The water vapor supply and total precipitation induced by LUCC become the primary factors influencing changes in mid-level and high-level clouds (Figure S13). Large-scale

https://doi.org/10.5194/egusphere-2026-367
Preprint. Discussion started: 8 May 2026

idealized afforestation causes insufficient water supply in the mid-to-high latitude regions of the NH, which also inhibits the development of CLDMED, but the impacts of bioenergy expansion and realistic afforestation are overall positive (Figure S17). More noteworthy are the high-level clouds that have a warming effect on the atmosphere; the increase in water vapor induced by large-scale idealized forest expansion leads to an increase in CLDHGH in the mid-to-high latitude regions of the NH, which may become an additional source of warming on the basis of mid- and low-level cloud loss (Lian et al., 2022). Therefore, idealized afforestation not only accelerates warming by accelerating the loss of mid- and low-level clouds, but also amplifies warming by promoting the increase of high-level clouds, and the warming induced by high-level clouds also exists in the bioenergy expansion and realistic afforestation simulations. In contrast, afforestation in real-world scenarios effectively optimizes the distribution of heat between the surface and the atmosphere, allowing atmospheric cooling and evapotranspiration efficiency (a positive manifestation of hydrothermal coupling) to dominate, successfully offsetting the warming effects caused by decreased albedo.

https://doi.org/10.5194/egusphere-2026-367
Preprint. Discussion started: 8 May 2026

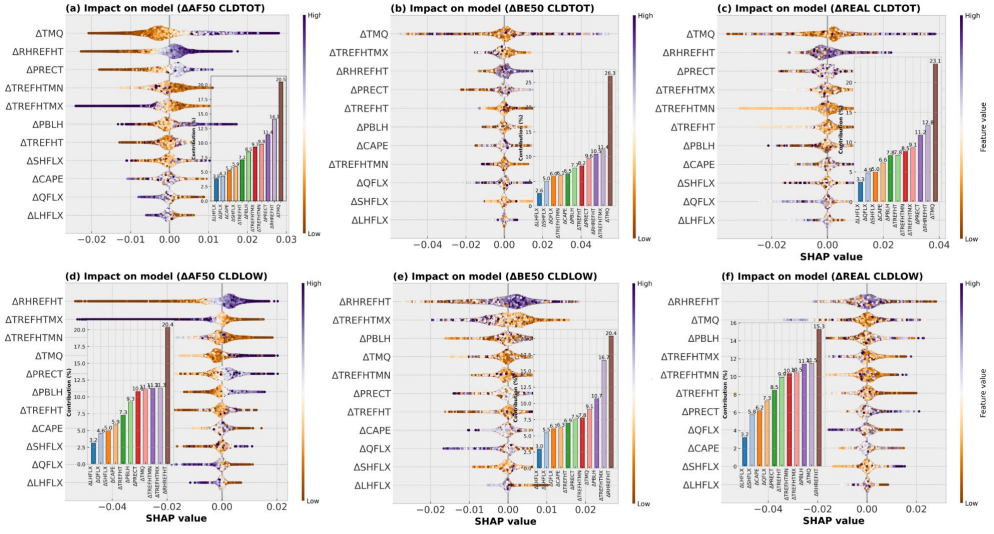

Figure 7. Drivers and contribution of CLDTOT and CLDLOW revealed by machine learning response to different land use change. Δ present the difference between sensitivity experiments and CTL. The contribution is expressed in SHapley Additive exPlanations (SHAP) value, which measure the impact of each driver factor induced by land use change on the model output (Berdugo et al., 2022). The bar chart shown in the illustration represents the percentage contribution. For CLDMED and CLDHGH can be viewed in Figure. S13. PRECT, total precipitation (mm/day); TMQ, total precipitable water (kg/m^2); TREFHT, air temperature at reference height (K); TREFHTMX, maximum temperature at reference height (K); RHREFHT, relative humidity at reference height (%); QFLX, evapotranspiration (mm/day); CAPE, convective available potential energy (J/kg); PBLH, planetary boundary layer height (m); TREFHTMN, minimum temperature at reference height (K); SHFLX, sensible heat flux (W/m^2); LHFLX, latent heat flux (W/m^2).

https://doi.org/10.5194/egusphere-2026-367
Preprint. Discussion started: 8 May 2026

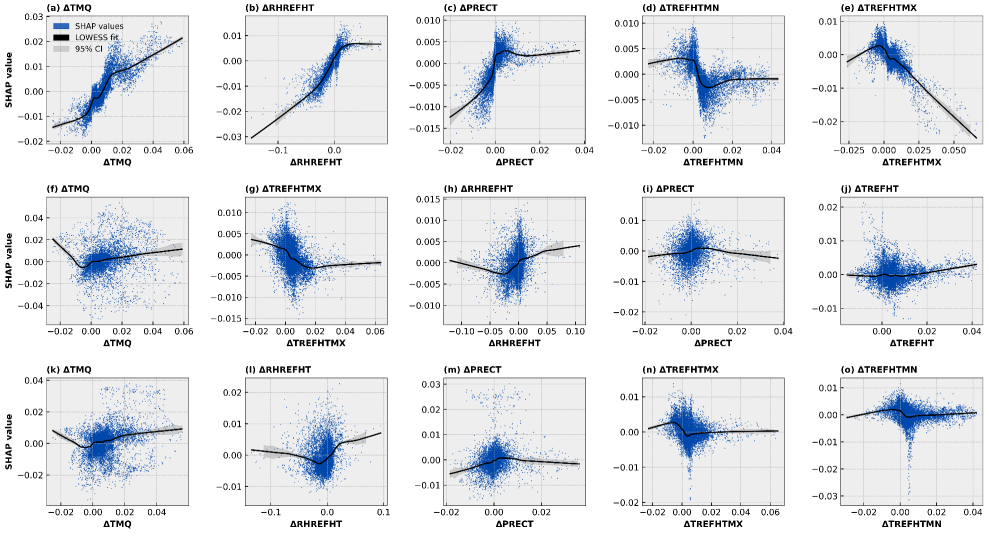

563

564 **Figure 8. Dependence plots of the top five important variables for total cloud cover**
565 **(CLDTOT), as revealed by the machine learning model.** The first to third rows represent
566 AF50, BE50 and REAL experiments respectively. SHAP dependence was visualized using
567 Locally Weighted Scatterplot Smoothing (LOWESS) (Cleveland. 1979) with a smoothing
568 fraction of frac=0.3 (using 30% of nearest neighbors for local regression) and it=3 robust
569 iterations to reduce outlier influence, and shaded band indicates 95% confidence interval
570 (CI) of LOWESS regression.

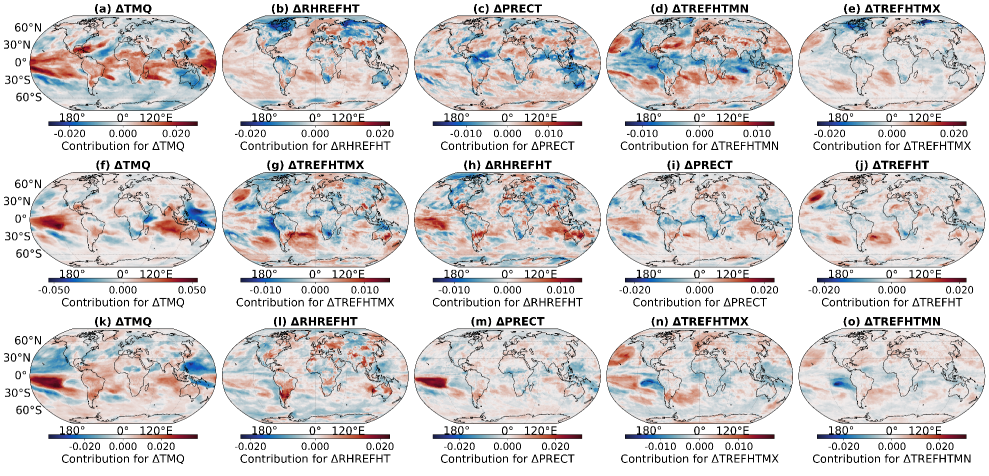

571

https://doi.org/10.5194/egusphere-2026-367
Preprint. Discussion started: 8 May 2026

Figure 9. Spatial drivers and contribution of CLDTOT revealed by machine learning response to different land use change. The first to third rows represent AF50, BE50 and REAL experiments respectively. The contribution is expressed in SHapley Additive exPlanations (SHAP) value.

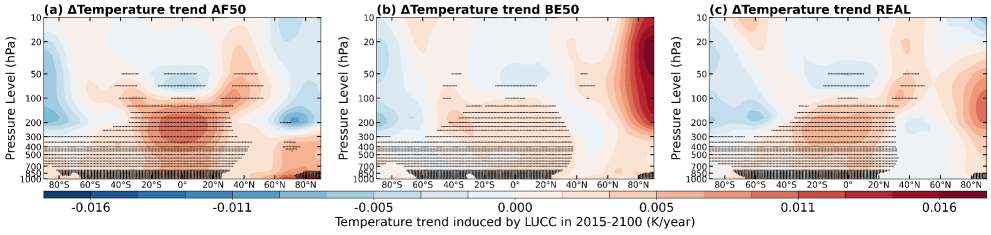

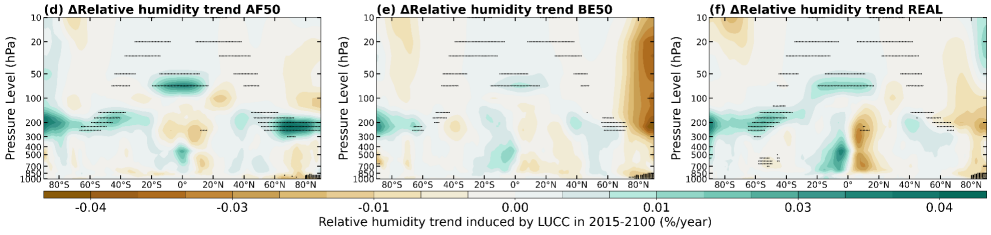

Figure 10. Trends in temperature and relative humidity induced by different LUCC at vertical heights. The black asterisk indicates the grids that passed the test of significance (p<0.05).

4. Discussions

Our simulation results indicate that two distinctly different future land use methods may significantly alter long-term cloud cover trends in terms of their impact on the magnitude of climate warming, particularly large-scale idealized forest expansion exacerbates cloud-mediated climate warming by substantially accelerating the loss of mid-low level clouds and the increase of high-level clouds. Bioenergy expansion also imposes negative impacts on cloud cover, but the overall intensity is weaker than that of idealized afforestation; this relatively mild negative impact may stem from lower LAI and reduced

https://doi.org/10.5194/egusphere-2026-367
Preprint. Discussion started: 8 May 2026

transpiration, as in previous assessments of this scheme, where bioenergy expansion may be accompanied by depletion of soil moisture and hinder the accumulation of atmospheric humidity (Le et al., 2011; Cheng et al., 2024). We believe that the negative impacts of these two large-scale idealized LUCC forcings on cloud cover originate from their own expansion areas, because in our simulations, the land for forest expansion is taken from grasslands or shrubs, which may lead to an increase in surface radiation absorption; the increased radiation warms the bottom of the convection layer in the form of sensible heat, thereby imposing more stringent conditions for cloud formation. In contrast, in the bioenergy expansion simulation (irrigated and rained sugarcane), the land comes from the land of other bioenergy crops, which means a reduction in the area of other crops with higher albedo, for example, switchgrass has an overall higher albedo than sugarcane and thus has greater climate cooling potential (Abraha et al., 2021; Lei et al., 2023). When other possible bioenergy crops with greater climate cooling potential are replaced by sugarcane, it may suppress cloud formation due to insufficient cooling, thereby inducing mild cloud loss. Furthermore, since our idealized afforestation scenarios involve converting grasslands or shrubs to forests, although this conforms to the Food and Agriculture Organization (FAO) definition (FAO. 2012), meaning our simulations are neither forest enhancement nor reforestation, it is also essential to consider the potential ecological consequences of such land type conversions. Grasslands, as one of the important terrestrial ecosystems, support unique biodiversity but are also relatively fragile; afforestation in these areas may lead to the loss of flora and fauna, reduced water availability, and increased fires (Veldman et al., 2015a; Veldman et al., 2015b; Parr et al., 2024). Therefore, although the primary goal of idealized afforestation is to enhance terrestrial carbon absorption, it carries the risk of

https://doi.org/10.5194/egusphere-2026-367
Preprint. Discussion started: 8 May 2026

ecological degradation (Cao. 2008; Xiao et al., 2020). Here, our idealized forest expansion simulation experiments are not intended to suggest implementing such forest expansion actions; on the contrary, the signal we are sending is cautionary.

On the other hand, we found that idealized and realistic afforestation suppressed the loss trends of total cloud and low-level cloud over the oceans, but idealized bioenergy expansion accelerated their loss trends (Figure S5). The question we need to answer here is actually through what pathways LUCC disturbances on land propagate energy to the oceans and influence cloud trends. According to previous simulation studies on deforestation, changes in albedo are considered the fundamental source of ocean responses; deforestation increases surface albedo, thereby reducing energy absorption at the surface, so no more heat is allocated to sensible heat flux to heat the convection layer, this process leads to cooling of the convection layer over the oceans (Davin and de Noblet-Ducoudré, 2010). In contrast, in our simulations, the albedo reduction caused by forest expansion (although not shown) induces the surface to absorb more solar radiation; the extra radiation is redistributed in the form of sensible heat flux to release into the atmosphere and heat the atmosphere, and the increased heat warms the ocean surface with ample moisture supply, making more water vapor condense into clouds. Therefore, forest expansion overall suppresses the loss rate of total cloud and low-level cloud cover in ocean areas.

Our hypothesis can be verified from Figure S20 and Figure S22, namely that forest expansion induces increasing trends in maximum temperature and total atmospheric precipitable water over the oceans. However, in bioenergy expansion, we observe overall opposite results (Figure S21), namely that bioenergy, due to relatively high albedo, does not lead to substantial warming of the oceans, thus there is not enough heat to make

https://doi.org/10.5194/egusphere-2026-367
Preprint. Discussion started: 8 May 2026

moisture evaporate and condense into clouds. In contrast, realistic afforestation overall does not render clouds detrimental to the climate; this difference largely stems from the type of land conversion and the regions involved. In idealized afforestation, forests are derived from grasslands or shrubs, with large amounts of C_3 grasslands distributed in mid-to-high latitude regions of the Northern Hemisphere and C_4 grasslands in tropical areas, whereas forest expansion in realistic afforestation simulations is not like this (Wei et al., 2014; Figure S23).

Due to the intrinsic uncertainties inherent in individual climate models, particularly concerning the simulation of cloud feedbacks (Ceppi et al., 2024), the evaluation of long-term impacts arising from external forcings such as land use and land cover change can often be robustly achieved through well-validated single-model simulations, as demonstrated in numerous prior studies (Snyder et al., 2004; Arora and Montenegro, 2011; Bauer et al., 2025). However, considering that CESM2 may be overly sensitive to aerosol-cloud interactions or thermal disturbances, the simulated cloud cover trend changes induced by LUCC may be an upper limit. While model ensembles or multi-model intercomparison frameworks have been employed to enhance confidence in conclusions (Falloon et al., 2014), they introduce limitations such as computational expense, potential overconfidence due to model dependence—where shared code, parameterizations, and biases among models undermine the assumption of independence (Abramowitz et al., 2019; Knutti et al., 2010)—and challenges in combining projections from a small or unevenly distributed set of models (von Trentini et al., 2020). Despite this, we still recommend, where computational resources permit, the integration of models with different equilibrium climate sensitivity (ECS) characteristics to adequately distinguish between signal and

https://doi.org/10.5194/egusphere-2026-367
Preprint. Discussion started: 8 May 2026

model structure biases (Khan et al., 2023). On the other hand, due to limitations in model resolution and cloud microphysical parameterization uncertainties (Morrison et al., 2020), which stem from incomplete representations of complex processes such as aerosol-cloud interactions, ice crystal formation, and precipitation efficiency, which can lead to substantial biases in simulated cloud optical properties and lifetime (Fan et al., 2016). These uncertainties often amplify errors in global climate projections, particularly regarding radiative forcing and feedback loops, highlighting the need for enhanced observational constraints and sensitivity analyses to refine model parameterizations. practical reforestation activities need to be guided by higher resolution and more accurate land cover data (Hoffmann et al., 2023), aiming for sufficient resolution to distinguish forests from other ecosystems. Our findings have profound implications for future land management and climate mitigation policies, highlighting that policymakers must move beyond a single carbon sequestration target and incorporate albedo risk into their decision-making framework, as previous studies have suggested (Wang et al., 2023), and also consider cloud-mediated climate risks.

5. Conclusions

We use the current state-of-the-art CESM to simulate the impact of two distinctly different future land use and cover changes (forest and bioenergy expansion) on long-term cloud cover trends. Simulation results show that future large-scale idealized forest and bioenergy expansions may exacerbate cloud-mediated regional climate warming, as they accelerate the loss of mid-low level clouds while enhancing the increase of high-level clouds, thereby diminishing the overall climate-regulating benefits of cloud cover. Specifically, idealized afforestation leads to the fastest low-level cloud loss (1.14 times on

https://doi.org/10.5194/egusphere-2026-367
Preprint. Discussion started: 8 May 2026

global, 1.52 times on land), followed by bioenergy expansion (1.03 times on global and 1.23 times on land), whereas realistic afforestation mitigates such losses and generates positive climate effects by preserving or enhancing cloud cover. The loss of mid-low level clouds amplifies the formation of regional warming hotspots through enhanced shortwave cloud radiative forcing trends, particularly in mid-to-high latitude regions of the Northern Hemisphere, where accelerated reductions in mid-low level cloud amounts align with amplified temperature trends (reaching up to 2.15 times the global average under idealized afforestation). The hemispheric asymmetry in cloud trends, quantified via Gini coefficients, further highlights how idealized forest and bioenergy expansions concentrate cloud loss trends within the latitudinal bands of those expansions, thereby potentially reshaping new climate warming hotspots. A coupled interpretable machine learning framework further elucidates the relevant mechanisms underlying cloud trend changes, emphasizing that the long-term decreasing trends in total atmospheric precipitable water and relative humidity induced by idealized forest and bioenergy expansions are the primary drivers of the accelerated loss of mid-low level clouds. These results underscore that not all forest expansions yield positive climate benefits; outcomes critically depend on the type of land conversion and the specific regions of implementation. This also highlights an important realization: even within bioenergy crops, the choice of crop function type is just as crucial as the choice of afforestation site. Therefore, policymakers should prioritize realistic afforestation strategies in suitable latitudinal zones to maximize carbon sequestration while avoiding unintended cloud-mediated warming.

Data availability

https://doi.org/10.5194/egusphere-2026-367
Preprint. Discussion started: 8 May 2026

All CESM simulation results and associated procedures are available on request from the authors. ERA5 data are available for download through the Copernicus Climate Service (https://cds.climate.copernicus.eu/datasets) (Muñoz-Sabater et al., 2021). National Centers for Environmental Prediction (NCEP) temperature is available from https://psl.noaa.gov/.

Author contribution

Nanjian Liu: Conceptualization, Methodology, Software, Formal analysis, Data curation, Visualization, Writing – original draft, Writing – review & editing.

Zhixin Hao: Conceptualization, Methodology, Funding acquisition, Supervision, Project administration, Writing – review & editing.

Siyou Xia: Writing – review & editing, Language polishing.

Peng Zhao: Software, Visualization, Writing – review & editing.

Competing interests

The authors declare that they have no known competing financial interests or personal relationships that could have appeared to influence the work reported in this paper.

Acknowledgments

This work was supported by the National Natural Science Foundation of China (Grant No. 42171030). We acknowledge the dendrochronology and paleoenvironmental analysis laboratory of the Institute of Geographic Sciences and Natural Resources Research, Chinese Academy of Sciences, for the computational support from its high-performance computing platform.

References

G. L. Stephens, Cloud Feedbacks in the Climate System: A Critical Review. J. Clim. 18, 237–273 (2005).

https://doi.org/10.5194/egusphere-2026-367
Preprint. Discussion started: 8 May 2026

726 N. G. Loeb, S H. Ham, R P. Allan, T J. Thorsen, B. Meyssignac, S. Kato, G C. Johnson, J
727 M. Lyman, Observational Assessment of Changes in Earth's Energy Imbalance
728 Since 2000. Surv Geophys 45, 1757–1783 (2024).
729 E. L. Davin, N. de Noblet-Ducoudré, Climatic impact of global-scale deforestation:
730 radiative versus non-radiative processes. J. Clim. 23, 97–112 (2010).
731 O. Boucher, D. Randall, P. Artaxo, C. Bretherton, G. Feingold, P. Forster, V.-M. Kerminen,
732 Y. Kondo, H. Liao, U. Lohmann, P. Rasch, S. K. Satheesh, S. Sherwood, B. Stevens,
733 and X.Y. Zhang, Clouds and aerosols. In Climate Change 2013: The Physical
734 Science Basis. (2013).
735 C. Lei, J. Chen, G. P. Robertson, Climate cooling benefits of cellulosic bioenergy crops
736 from elevated albedo. Glob. Change Biol. Bioenergy. 15(11), 13098 (2023).
737 S. Cao. Why large-scale afforestation efforts in China have failed to solve the
738 desertification problem. Environ. Sci. Technol. 42(6), 1826–1831 (2008).
739 Y. Xiao, Q. Xiao, X. Sun. Ecological risks arising from the impact of large-scale
740 afforestation on the regional water supply balance in southwest China. Sci. Rep. 10,
741 4150 (2020).
742 M. Abraha, J. Chen, S. K. Hamilton, P. Sciusco, C. Lei, G. Shirkey, J. Yuan & G. P.
743 Robertson, Albedo-induced global warming impact of Conservation Reserve
744 Program grasslands converted to annual and perennial bioenergy crops. Environ.
745 Res. Lett. 16, 084059 (2021).
746 G. Tselioudis, W. B. Rossow, F. Bender, L. Oreopoulos, J. Remillard, Oceanic cloud trends
747 during the satellite era and their radiative signatures. Clim Dyn. 62, 9319–9332
748 (2024).

https://doi.org/10.5194/egusphere-2026-367
Preprint. Discussion started: 8 May 2026

749 J. Foley, R. Defries, G. Asner, C. Barford, G. Bonan, S. Carpenter, F. Chapin, M. Coe, G.
750 Daily, H. Gibbs, J. Helkowski, T. Holloway, E. Howard, C. Kucharik, C. Monfreda,
751 A. Patz, I. Prentice, N. Ramankutty, P. Snyder, Global consequences of land use.
752 Science. 309(5734), 570–574 (2005).
753 X. Q. Li, Q X. Li, M. Wild, P. Jones, An intensification of surface Earth's energy imbalance
754 since the late 20th century. Commun Earth Environ. 5, 644 (2024).
755 R. Portmann, U. Beyerle, E. Davin, E. M. Fischer, S. De Hertog, S. Schemm, Global
756 forestation and deforestation affect remote climate via adjusted atmosphere and
757 ocean circulation. Nat. Commun. 13, 1–11 (2022).
758 W. Hua, L. Zhou, A. Dai, H. Chen, and Y. Liu, Important non-local effects of deforestation
759 on cloud cover changes in CMIP6 models, Environ. Res. Lett. 18, 094047 (2023).
760 J. R.Taylor. An Introduction to Error Analysis: The Study of Uncertainties in Physical
761 Measurements [M]. 2nd ed. Sausalito: University Science Books. (1997).
762 P. Hoffmann, V. Reinhart, D. Rechid, N. de Noblet-Ducoudré, E. L. Davin, C. Asmus, B.
763 Bechtel, J. Böhner, E. Katragkou, S. Luyssaert. High-resolution land use and land
764 cover dataset for regional climate modelling: historical and future changes in
765 Europe. Earth Syst. Sci. Data 15, 3819–3852 (2023).
766 G. R. Leung, L. D. Grant, S. C. van den Heever. Deforestation-Driven Increases in Shallow
767 Clouds Are Greatest in Drier, Low-Aerosol Regions of Southeast Asia. Geophys.
768 Res. Lett. 51(10), e2023GL107678 (2024).
769 M. D. Mastrandrea, C. B. Field, T. F. Stocker, O. Edenhofer, K. L. Ebi, D. J. Frame, H.
770 Held, E. Kriegler, K. J. Mach, P. R. Matschoss, G.-K. Plattner, G. W. Yohe, F. W.
771 Zwiers, Guidance Note for Lead Authors of the IPCC Fifth Assessment Report on

https://doi.org/10.5194/egusphere-2026-367
Preprint. Discussion started: 8 May 2026

Consistent Treatment of Uncertainties (Intergovernmental Panel on Climate Change, 2010).

H. Morrison, M. van Lier-Walqui, A. M. Fridlind, W. W. Grabowski, J. Y. Harrington, C. Hoose, A. Korolev, H. E. Kumjian, J. A. Milbrandt, H. Pawlowska, D. P. Posselt, A. Prabhakaran, K. Shima, B. A. van Diedenhoven, L. Xue. Confronting the Challenge of Modeling Cloud and Precipitation Microphysics. J. Adv. Model. Earth Syst. 12(8), e2019MS001689 (2020).

A. J. Teuling, C. M. Taylor, J. F. Meirink, L. A. Melsen, D. G. Miralles, C. C. van Heerwaarden, R. Vautard, A. I. Stegehuis, G.-J. Nabuurs & J. Vilà-Guerau de Arellano, Observational evidence for cloud cover enhancement over western European forests. Nat. Commun. 8, 14065 (2017).

M. Ek, A. A. M. Holtslag, Influence of soil moisture on boundary layer cloud development. J. Hydrometeorol. 5, 86–99 (2004).

J. J. Feddema, K. W. Oleson, G. B. Bonan, L. O. Mearns, L. E. Buja, G. A. Meehl, W. M. Washington, The Importance of Land-Cover Change in Simulating Future Climates. Science. 310(5754), 1674–1678.

T. Mauritsen, Earth's Energy Imbalance More Than Doubled in Recent Decades. AGU Advances. 6(3), e2024AV001636 (2025).

G. Duveiller, F. Filipponi, A. Ceglar, J. Bojanowski, R. Alkama, A. Cescatti, Revealing the widespread potential of forests to increase low level cloud cover. Nat Commun. 12, 4337 (2021).

P. K. Snyder, C. Delire, J. A. Foley. Evaluating the influence of different vegetation biomes on the global climate. Clim.Dyn. 23,279-302 (2004).

https://doi.org/10.5194/egusphere-2026-367
Preprint. Discussion started: 8 May 2026

W. S. Cleveland. Robust Locally Weighted Regression and Smoothing Scatterplots. Journal of the American Statistical Association. 74(368),829-836.

K. N. Liou, S. C. Ou, Theory of equilibrium temperatures in radiative-turbulent atmospheres. J. Atmos. Sci. 40,214–229 (1983).

R. A. Houghton, The annual net flux of carbon to the atmosphere from changes in land use 1850–1990. 51(2), 298–313 (2002).

K. K. Goldewijk, N. Ramankutty, Land cover change over the last three centuries due to human activities: The availability of new global data sets. GeoJournal. 61, 335–344 (2004).

C. Goldblatt, V.L. McDonald, K.E. McCusker, Earth's long-term climate stabilized by clouds. Nat. Geosci. 14, 143–150 (2021).

Y. Cheng, D. M. Lawrence, M. Pan, B. Zhang, N. T. Graham, P J. Lawrence, Z. Liu, X. He, A bioenergy-focused versus a reforestation-focused mitigation pathway yields disparate carbon storage and climate responses, Proc. Natl. Acad. Sci. 121 (7), e2306775121 (2024).

S. Peng, S. Piao, Z. Zeng, P. Ciais, L. Zhou, L. Z. X. Li, R. B. Myneni, Y. Yin, H. Zeng, Afforestation in China cools local land surface temperature. Proc. Natl. Acad. Sci. 111 (8), 2915-2919 (2014).

J. Fan, Y. Wang, D. Rosenfeld, X. Liu, Review of aerosol–cloud interactions: Mechanisms, significance, and challenges. J. Atmos. Sci. 73(11), 4221-4252 (2016)

K. Oleson, D. Lawrence, G.B. Bonan, Technical description of version 4.5 of the Community Land Model (CLM). NCAR Tech. Note NCAR/TN-503+STR. National Center for Atmospheric Research, Boulder. 2013.

https://doi.org/10.5194/egusphere-2026-367
Preprint. Discussion started: 8 May 2026

818 Y. Cheng, M. Huang, D. M. Lawrence, K. Calvin, D. L. Lombardozzi, E. Sinha, M. Pan,
819 X. He, Future bioenergy expansion could alter carbon sequestration potential and
820 exacerbate water stress in the United States. Sci. Adv.8,eabm8237(2022).
821 W. Hallgren, C. A. Schlosser, E. Monier, D. Kicklighter, A. Sokolov, J. Melillo, Climate
822 impacts of a large-scale biofuels expansion. Geophys. Res. Lett. 40(8), 1624–1630
823 (2013).
824 A. L. Swann, I. Y. Fung, S. Levis, G. B. Bonan, S. C. Doney, Changes in Arctic vegetation
825 amplify high-latitude warming through the greenhouse effect. Proc. Natl. Acad. Sci.
826 U.S.A. 107, 1295–1300 (2010).
827 G. Bala, K. Caldeira, M. Wickett, T J. Phillips, D B. Lobell, C. Delire, A. Mirin, Combined
828 climate and carbon-cycle effects of large-scale deforestation. Proc. Natl. Acad. Sci.
829 104, 6550–6555 (2007).
830 M. Georgescu, D.B. Lobell, C.B. Field, Direct climate effects of perennial bioenergy crops
831 in the United States. Proc. Natl. Acad. Sci. 108 (11) 4307–4312 (2011).
832 Z. Li, P. Ciais, J. S. Wright, Y. Wang, S. Liu, J. Wang, L. Z. X. Li, H. Lu, X. Huang, L.
833 Zhu, D. S. Goll, W. Li, Increased precipitation over land due to climate feedback
834 of large-scale bioenergy cultivation. Nat Commun. 14, 4096 (2023).
835 G. van der Werf, D. Morton, R. DeFries et al., CO_2 emissions from forest loss. Nature
836 Geosci. 2, 737–738 (2009).
837 J. Wang, W. Li, P. Ciais, L. Z. X. Li, J. Chang, D. Goll, T. Gasser, X. Huang, N. Devaraju,
838 O. Boucher, Global cooling induced by biophysical effects of bioenergy crop
839 cultivation. Nature Commun. 7255 (2021).

https://doi.org/10.5194/egusphere-2026-367
Preprint. Discussion started: 8 May 2026

840 H. F. Goessling T. Rackow, T. Jung, Recent global temperature surge intensified by record-
841 low planetary albedo. Science. 387,68–73 (2025).
842 S. A. Klein, A. Hall, J. R. Norris, R. Pincus, Low-Cloud Feedbacks from Cloud-Controlling
843 Factors: A Review. Surv Geophys. 38, 1307–1329 (2017).
844 C. L. Boehm, D. W. J. Thompson, The key role of cloud–climate coupling in extratropical
845 sea surface temperature variability. J. Clim. 36, 2753–2762 (2023).
846 J. T. Kiehl, Twentieth century climate model response and climate sensitivity. Geophys.
847 Res. Lett. 34, L22710 (2007).
848 C. Shi, T. Wang, G. Wang, H. Letu, The net warming effect of clouds on global surface
849 temperature may be weakening or even disappearing. GEOSCI FRONT. 16(5),
850 102107(2025).
851 S. M. Lundberg, S. -I. I. Lee, A unified approach to interpreting model predictions.
852 Advances in Neural Information Processing Systems. 2017-Decem(Section 2),
853 4766–4775(2017).
854 P. V. V. Le, P. Kumar, D. T. Drewry. Implications for the hydrologic cycle under climate
855 change due to the expansion of bioenergy crops in the Midwestern United States.
856 Proc. Natl. Acad. Sci. U.S.A. 108 (37), 15085-15090 (2011).
857 A. L. S. Swann, I Y. Fung, J C H. Chiang, Mid-latitude afforestation shifts general
858 circulation and tropical precipitation. Proc. Natl. Acad. Sci. 109 (3), 712–716,
859 (2012).
860 M. Breil, V. K. M. Schneider, J. G. Pinto, The effect of forest cover changes on the regional
861 climate conditions in Europe during the period 1986–2015. Biogeosciences. 21,
862 811–824 (2024).

https://doi.org/10.5194/egusphere-2026-367
Preprint. Discussion started: 8 May 2026

863 Y. Li, S. Piao, L. Z. X. Li, A. Chen, X. Wang, P. Ciais, L. Huang, X. Lian, S. Peng, Z.
864 Zeng, K. Wang, L. Zhou, Divergent hydrological response to large-scale
865 afforestation and vegetation greening in China. Sci. Adv.4,eaar4182 (2018).
866 R. Righelato, D. V. Spracklen, Carbon mitigation by biofuels or by saving and restoring
867 forests? Science 317, 902 (2007).
868 M. M. Laguë Abigail L. S. Swann, Progressive Midlatitude Afforestation: Impacts on
869 Clouds, Global Energy Transport, and Precipitation. J.Clim. 29(15),5561–
870 5573(2016).
871 S. Liang, A D. Ziegler, P B. Reich, K. Zhu, D. Wang, X. Jiang, D. Chen, P. Ciais, Climate
872 mitigation potential for targeted forestation after considering climate change, fires,
873 and albedo. Sci. Adv.11,eadn7915 (2025).
874 T. Nomokonova, K. Ebell, U. Löhnert, M. Maturilli, C. Ritter, The influence of water vapor
875 anomalies on clouds and their radiative effect at Ny-Ålesund. Atmos. Chem. Phys.
876 20(8), 5157–5173 (2020).
877 P. H. Worley, A. P. Craig, J. M. Dennis, A. A. Mirin, M. A. Taylor, M. Vertenstein,
878 Performance and Performance Engineering of the Community Earth System Model.
879 Lawrence Livermore National Laboratory. 2011.
880 E. Kutta, J. A. Hubbart, Seasonal Lifting Condensation Level Trends: Implications of
881 Warming and Reforestation in Appalachia's Deciduous Forest. Atmosphere 14 (1),
882 98 (2023).
883 D. M. Romps, Exact Expression for the Lifting Condensation Level. J. Atmos. Sci. 74 (12),
884 3891–3900 (2017).

https://doi.org/10.5194/egusphere-2026-367
Preprint. Discussion started: 8 May 2026

C. Hong, J. A. Burney, J. Pongratz, J. E. M. S. Nabel, N. D. Mueller, R. B. Jackson ,S. J. Davis, Global and regional drivers of land-use emissions in 1961–2017. Nature. 589, 554–561 (2021).

S. Cerasoli, J. Yin, A. Porporato, Cloud cooling effects of afforestation and reforestation at midlatitudes. Proc. Natl. Acad. Sci. U.S.A. 118(33), e2026241118 (2021).

J. Wang, W. Li, P. Ciais, L. Z. X. Li, J. Chang, D. Goll, T. Gasser, X. Huang, N. Devaraju, O. Boucher. Global cooling induced by biophysical effects of bioenergy crop cultivation. Nat. Commun. 12, 7255 (2021).

Y. Li, B. Huang, C. Tan, X. Zhang, Investigating the global and regional response of drought to idealized deforestation using multiple global climate models. Hydrology and Earth System Sciences. 29, 1637-1658 (2025).

X. Lian, S. Jeong, C.-E. Park, H. Xu, L. Z. X. Li, T. Wang, P. Gentine, J. Peñuelas, S. Piao. Biophysical impacts of northern vegetation changes on seasonal warming patterns. Nat Commun. 13, 3925 (2022).

J. A. King, J Weber, P Lawrence, S. Roe, A. L. S. Swann, M. Val Martin, Global and regional hydrological impacts of global forest expansion. JGR-Biogeosciences. 21(17), 3883–3902 (2024).

H. Zhao, M. Manizza, M. S. Lozier, N. Cassar. Greener green and bluer blue: Ocean poleward greening over the past two decades. Science. 388(6753), 1337–1340 (2025).

N. Khan, M. A. Nasara, Z. Sa'adi, D. P. Awhari, M. I. Asiri, S. Shahid, Z. M. Yaseen. Global climate models performance: A comprehensive review of applied

https://doi.org/10.5194/egusphere-2026-367
Preprint. Discussion started: 8 May 2026

approaches, recognized issues and possible future directions. Atmos. Res. 326, 108300 (2025).

M. Berdugo, J.J. Gaitán, M. Delgado-Baquerizo, T.W. Crowther, V. Dakos, Prevalence and drivers of abrupt vegetation shifts in global drylands, Proc. Natl. Acad. Sci. 119 (43), e2123393119 (2022).

C. Zhou, M. Zelinka, S. Klein, Impact of decadal cloud variations on the Earth's energy budget. Nature Geosci. 9, 871–874 (2016).

H. Zhang, F. Wang, F. Wang, J. Li, X. Chen, Z. Wang, J. Li, X. Zhou, Q. Wang, H. Wang, T. You, B. Xie, Q. Chen, Y. Duan. Advances in cloud radiative feedbacks in global climate change (in Chinese). Scientia Sinica Terrae, 52(3), 400–417 (2022).

M. D. Zelinka, C. Zhou, S. A. Klein, Insights from a refined decomposition of cloud feedbacks. Geophys. Res. Lett. 43(17),9259-9269(2016).

P. Ceppi, P. Nowack, Observational evidence that cloud feedback amplifies global warming. Proc. Natl. Acad. Sci. 118 (30), e2026290118 (2021).

L. Liu, Y. Huang, J. R. Gyakum, Clouds reduce downwelling longwave radiation over land in a warming climate. Nature. 637, 868–874 (2025).

R. A. Pielke Sr, J. Adegoke, A. Beltrán-Przekurat, C. A. Hiemstra, J. Lin, U. S. Nair, D. Niyogi, and T. E. Nobis. An overview of regional land-use and land-cover impacts on rainfall. Tellus B. 59 (3), 587–601 (2007).

X. Lee, M. L. Goulden, D. Y. Hollinger, A. Barr, T. A. Black, G. Bohrer, R. Bracho, B. Drake, A. Goldstein, L. Gu, G. Katul, T. Kolb, B. E. Law, H. Margolis, T. Meyers, R. Monson, W. Munger, R. Oren, K. T. Paw U, A. D. Richardson, H. P. Schmid,

https://doi.org/10.5194/egusphere-2026-367
Preprint. Discussion started: 8 May 2026

R. Staebler, S. Wofsy, L. Zhao, Observed increase in local cooling effect of deforestation at higher latitudes. Nature. 479(7373),384-387(2011).

V. M. Bauer, S. Schemm, R. Portmann, J. Zhang, G. K. Eirund, S. J. De Hertog, J. Zibell. Impacts of North American forest cover changes on the North Atlantic Ocean circulation. Earth. Syst. Dyn. 16(2),16,379-409 (2025).

S. H. Schneider, Cloudiness as a Global Climatic Feedback Mechanism: The Effects on the Radiation Balance and Surface Temperature of Variations in Cloudiness. J ATMOS SCI. 29(8), 1413-1422 (1972).

M. Breil, E. L. Davin, D. Rechid. What determines the sign of the evapotranspiration response to afforestation in European summer? Biogeosciences. 18(4), 1499-1510 (2021).

J. A. Foley, J. E. Kutzbach, M. T. Coe, S. Levis, Feedbacks between climate and boreal forests during the Holocene epoch. Nature. 371, 52–54 (1994).

M. D. Zelinka, D. A. Randall, M. J. Webb, S. A. Klein, Clearing clouds of uncertainty. Nature Clim Change. 7, 674–678 (2017).

J. Weber, J. A. King, N. L. Abraham, D. P. Grosvenor, C. J. Smith, Y. M. Shin, P. Lawrence, S. Roe, D. J. Beerling, M. Val Martin. Chemistry-albedo feedbacks offset up to a third of forestation's CO2 removal benefits. Science. 383 (6685), 860-864 (2024).

B. A. Albrecht, Aerosols. cloud microphysics and fractional cloudiness. Science. 245, 1227–1230 (1989).

G. Duveiller, J. Hooker, A. Cescatti, The mark of vegetation change on Earth's surface energy balance. Nature Commun. 9(1), 679 (2018).

https://doi.org/10.5194/egusphere-2026-367
Preprint. Discussion started: 8 May 2026

951 R. Alkama, A, Cescatti, Biophysical climate impacts of recent changes in global forest
952 cover. Science. 351(6273), 600–604 (2016).
953 H. Luo, J. Quaas, Y. Han, Diurnally asymmetric cloud cover trends amplify greenhouse
954 warming. Sci. Adv.10, eado5179(2024).
955 T. Nomokonova, K. Ebell, U. Löhnert, M. Maturilli, C. Ritter, The influence of water vapor
956 anomalies on clouds and their radiative effect at Ny-Ålesund. ATMOS CHEM
957 PHYS. 20(8), 5157-5173 (2020).
958 G. Tselioudis, J. Remillard, C. Jakob, W. B. Rossow, Contraction of the World's Storm-
959 Cloud Zones the Primary Contributor to the 21st Century Increase in the Earth's
960 Sunlight Absorption. Geophys. Res. Lett. 52(11), e2025GL114882(2025).
961 C. Chen, L. Wang, R. B. Myneni, D. Li, Attribution of Land-Use/Land-Cover Change
962 Induced Surface Temperature Anomaly: How Accurate Is the First-Order Taylor
963 Series Expansion?. JGR Biogeosciences. 125(9),e2020JG005787(2020).
964 G. Danabasoglu, J. F. Lamarque, J. Bacmeister, D. A. Bailey, A. K. DuVivier, J. Edwards,
965 L. K. Emmons, J. Fasullo, R. Garcia, A. Gettelman, C. Hannay, M. M. Holland, W.
966 G. Large, P. H. Lauritzen, D. M. Lawrence, J. T. M. Lenaerts, K. Lindsay, W. H.
967 Lipscomb, M. J. Mills, R. Neale, K. W. Oleson, B. Otto-Bliesner, A. S. Phillips, W.
968 Sacks, S. Tilmes, L. van Kampenhout, M. Vertenstein, A. Bertini, J. Dennis, C.
969 Deser, C. Fischer, B. Fox-Kemper, J. E. Kay, D. Kinnison, P. J. Kushner, V. E.
970 Larson, M. C. Long, S. Mickelson, J. K. Moore, E. Nienhouse, L. Polvani, P. J.
971 Rasch, W. G. Strand, The Community Earth System Model Version 2 (CESM2). J.
972 Adv. Model. Earth Syst. 12(2), e2019MS001916 (2020).

https://doi.org/10.5194/egusphere-2026-367
Preprint. Discussion started: 8 May 2026

973 J. T. Fasullo. Evaluating simulated climate patterns from the CMIP archives using satellite
974 and reanalysis datasets using the Climate Model Assessment Tool (CMATv1).
975 Geosci. Model Dev. 13, 3627–3642 (2020).
976 J. Zhu, B. L. Otto-Bliesner, E. C. Brady, A. Gettelman, J. T. Bacmeister, R. B. Neale, C. J.
977 Poulsen, J. K. Shaw, Z. S. McGraw, J. E. Kay. LGM Paleoclimate Constraints
978 Inform Cloud Parameterizations and Equilibrium Climate Sensitivity in CESM2. J.
979 Adv. Model. Earth Syst. 14(4), e2021MS002776 (2022).
980 S. J. Lin, R. B. Rood, An explicit Flux-Form Semi-Lagrangian shallow water model on the
981 sphere. Quarterly Q. J. R. Meteorol. Soc. 123, 2477–2498 (1997).
982 H. Morrison, A. Gettelman, A new two-moment bulk stratiform cloud microphysics
983 scheme in the NCAR community atmosphere model (CAM3), Part I: Description
984 and numerical tests. J. Clim, 21, 3642–3659 (2008).
985 A. Gettelman, H. Morrison, Advanced two-moment bulk microphysics for global models.
986 Part I: Off-line tests and comparison with other schemes. J. Clim. 28, 1268–1287
987 (2015).
988 V. E. Larson, CLUBB-SILHS: A parameterization of subgrid variability in the atmosphere.
989 2017.
990 N. Devaraju, Nathalie de Noblet-Ducoudré, Benjamin Quesada, G. Bala, Quantifying the
991 relative importance of direct and indirect biophysical effects of deforestation on
992 surface temperature and teleconnections. J.Clim. 31(10), 3811-3829(2018).
993 Y. Sui, M. Wei, B. Liu, Biophysical Impacts of Global Deforestation on Near-Surface Air
994 Temperature in China: Results from Land Use Model Intercomparison Project
995 Simulations. Adv. Atmos. Sci., 42, 1141-1155(2025).

https://doi.org/10.5194/egusphere-2026-367
Preprint. Discussion started: 8 May 2026

996 K. J. Meissner, A. J. Weaver, H. D. Matthews, P. M. Cox, The role of land surface
997 dynamics in glacial inception: a study with the UVic Earth System Model. Climate
998 Dynamics. 21, 515–537(2003).
999 V. Arora, Montenegro, Small temperature benefits provided by realistic afforestation
1000 efforts. Nature Geosci. 4, 514–518(2011).
1001 S. C. Swenson, D. Lawrence, A new fractional snow-covered area parameterization for the
1002 Community Land Model and its effect on the surface energy balance. J GEOPHYS
1003 RES-ATMOS. 117, D21107 (2012).
1004 D. M. Lawrence, R. A. Fisher, C. D. Koven, K. W. Oleson, S. C. Swenson, G. Bonan, N.
1005 Collier, B. Ghimire, L. van Kampenhout, D. Kennedy, E. Kluzek, P. J. Lawrence,
1006 F. Li, H. Li, D. Lombardozzi, W. J. Riley, W. J. Sacks, M. Shi, M. Vertenstein, W.
1007 R. Wieder, C. Xu, A. A. Ali, A. M. Badger, G. Bisht, M. van den Broeke, M. A.
1008 Brunke, S. P. Burns, J. Buzan, M. Clark, A. Craig, K. Dahlin, B. Drewniak, J. B.
1009 Fisher, M. Flanner, A. M. Fox, P. Gentine, F. Hoffman, G. Keppel-Aleks, R. Knox,
1010 S. Kumar, J. Lenaerts, L. R. Leung, W.H. Lipscomb, Y. Lu, A. Pandey, J. D.
1011 Pelletier, J. Perket, J. T. Randerson, D. M. Ricciuto, B. M. Sanderson, A. Slater, Z.
1012 M. Subin, J. Tang, R.Q. Thomas, M. Val Martin, X. Zeng, The Community Land
1013 Model Version 5: Description of New Features, Benchmarking, and Impact of
1014 Forcing Uncertainty. J. Adv. Model. Earth Syst. 11(12), 4245–4287 (2019).
1015 G. C. Hurtt, L. Chini, R. Sahajpal, S. Frolking, B. L. Bodirsky, K. Calvin, J. C. Doelman,
1016 J. Fisk, S. Fujimori, K. Klein Goldewijk, T. Hasegawa, P. Havlik, A. Heinimann,
1017 F. Humpenöder, J. Jungclaus, J. O. Kaplan, J. Kennedy, T. Krisztin, D. Lawrence,
1018 P. Lawrence, L. Ma, O. Mertz, J. Pongratz, A. Popp, B. Poulter, K. Riahi, E.

https://doi.org/10.5194/egusphere-2026-367
Preprint. Discussion started: 8 May 2026

Shevliakova, E. Stehfest, P. Thornton, F. N. Tubiello, D. P. van Vuuren, X. Zhang, Harmonization of global land use change and management for the period 850–2100 (LUH2) for CMIP6. Geosci. Model Dev. 13, 5425–5464 (2020).

T. Chen, C. Guestrin, XGBoost: a scalable tree boosting system. In Proceedings of the 22nd ACM SIGKDD International Conference on Knowledge Discovery and Data Mining, San Francisco, California, USA. 785-794 (2016).

P. Falloon, A. Challinor, S. Dessai, L. Hoang, J. Johnson, A.-K. Koehler. Ensembles and uncertainty in climate change impacts. Front. Environ. Sci. 2, 33 (2014).

G. Abramowitz, N. Herger, E. Gutmann, D. Hammerling, R. Knutti, M. Leduc, R. Lorenz, R. Pincus, G. A. Schmidt. ESD Reviews: Model dependence in multi-model climate ensembles: weighting, sub-selection and out-of-sample testing. Earth Syst. Dynam. 10(1), 91–105 (2019).

R. Knutti, R. Furrer, C. Tebaldi, J. Cermak, and G. A. Meehl. Challenges in combining projections from multiple climate models. J. Clim. 23(10), 2739–2758 (2010).

F. von Trentini, E. E. Aalbers, E. M. Fischer, and R. Ludwig. Comparing interannual variability in three regional single-model initial-condition large ensembles (SMILEs) over Europe. Earth Syst. Dynam. 11(4), 1013–1031 (2020).

J. Snoek, H. Larochelle, R. P. Adams. Practical Bayesian Optimization of Machine Learning Algorithms. Advances in Neural Information Processing Systems. 25, 2960-2968 (2012).

Y. Wei, S. Liu, D. N. Huntzinger, A. M. Michalak, N. Viovy, W. M. Post, C. R. Schwalm, K. Schaefer, A. R. Jacobson, C. Lu, H. Tian, D. M. Ricciuto, R. B. Cook, J. Mao, and X. Shi, The North American Carbon Program Multi-scale Synthesis and

https://doi.org/10.5194/egusphere-2026-367
Preprint. Discussion started: 8 May 2026

Terrestrial Model Intercomparison Project – Part 2: Environmental driver data, Geosci. Model Dev., 7, 2875–2893(2014).

Y. Ren, J. Qiu, Z. Zeng, X. Liu, S. Sitch, K. Pilegaard, T. Yang, S. Wang, W. Yuan, A. K. Jain. Earlier spring greening in Northern Hemisphere terrestrial biomes enhanced net ecosystem productivity in summer. Commun Earth Environ. 5, 122 (2024).

S. M. Lundberg, G. Erion, H. Chen, A. DeGrave, J. M. Prutkin, B. Nair, R. Katz, J. Himmelfarb, N. Bansal, S. -I. Lee, From local explanations to global understanding with explainable AI for trees. Nat. Mach. Intell. 2, 56–67 (2020).

J. Muñoz-Sabater, E. Dutra, C. Agustí-Panareda, G. Albergel, G. Arduini, S. Balsamo, M. Boussetta, S. Choulga, H. Harrigan, H. Hersbach, D. Martens, M. Miralles, N. Piles, E. Rodríguez-Fernández, C. Zsoter, J. Buontempo, J.-N. Thépaut. ERA5-Land: A state-of-the-art global reanalysis dataset for land applications. Earth Syst. Sci. Data. 13 (9), 4349-4383 (2021).

C. L. Parr, M. te Beest, N. Stevens, Conflation of reforestation with restoration is widespread. Science. 383(6684),698-701.

FAO FRA. Forest Resources Assessment 2015: Terms and Definitions. FAO Rep. 36, (2012).

J. Weber, J. A. King, N. L. Abraham, D. P. Grosvenor, C. J. Smith, Y. M. Shin, P. Lawrence, S. Roe, D. J. Beerling, M. Val Martin, Chemistry-albedo feedbacks offset up to a third of forestation's CO2 removal benefits. Science, 2024, 383(6685), 860–864 (2024)

https://doi.org/10.5194/egusphere-2026-367
Preprint. Discussion started: 8 May 2026

1063 K. Wang, D. Zhao, Y. Zhu, X. Gao, S. Deng, Z. Chen, S. Wang, Y. Cui, Albedo-dominated
1064 biogeophysical warming effects induced by vegetation restoration on the Loess
1065 Plateau, China. Ecol Indic. 154,110690(2023).
1066 J. W. Veldman, G. E. Overbeck, D. Negreiros, G. Mahy, S. Le Stradic, G. W. Fernandes,
1067 G. Durigan, E. Buisson, F. E. Putz, W. J. Bond, Tyranny of trees in grassy biomes.
1068 Science. 347(6221),484-485(2015a).
1069 J. W. Veldman, G. E. Overbeck, D. Negreiros, G. Mahy, S. Le Stradic, G. W. Fernandes,
1070 G. Durigan, E. Buisson, F. E. Putz, W. J. Bond, Where Tree Planting and Forest
1071 Expansion are Bad for Biodiversity and Ecosystem Services. BioScience.
1072 65(10),1011-1018(2015b).
1073 M. L. Flora, C. K. Potvin, A. McGovern & S. Handler, A Machine Learning Explainability
1074 Tutorial for Atmospheric Sciences. Artificial Intelligence for the Earth Systems.
1075 e230018 (2024).
1076 S. Roe, C. Streck, R. Beach, J. Busch, M. Chapman, V. Daioglou, A. Deppermann, J.
1077 Doelman, J. Emmet-Booth, J. Engelmann, O. Fricko, C. Frischmann, J. Funk, G.
1078 Grassi, B. Griscom, P. Havlik, S. Hanssen, F. Humpenöder, D. Landholm, G.
1079 Lomax, J. Lehmann, L. Mesnildrey, G.-J. Nabuurs, A. Popp, C. Rivard, J.
1080 Sanderman, B. Sohngen, P. Smith, E. Stehfest, D. Woolf, D. Lawrence, Land-
1081 based measures to mitigate climate change: Potential and feasibility by country,
1082 Glob. Change Biol. 27, 6025–6058 (2021).